Thesis for the degree of Doctor of Philosophy

The data perspective on chiral effective field theory

Boris D. Karlsson

Department of Physics
Chalmers University of Technology
Gothenburg, Sweden 2017

The data perspective on chiral effective field theory
Boris D. Karlsson
ISBN 978-91-7597-530-6

Doktorsavhandlingar vid Chalmers tekniska högskola
Ny serie nr. 4211
ISSN 0346-718X
Department of Physics
Chalmers University of Technology
SE-412 96 Gothenburg
Sweden
Telephone: +46 (0)31-772 1000

Cover:
The total elastic neutron-proton scattering cross section as a function of the scattering energy. The uncertainty bands, from broad to thin, represent increasingly accurate predictions using chiral effective field theory when moving from the leading order approximation up to the fourth order approximation.

Chalmers Reproservice
Gothenburg, Sweden 2017

The data perspective on chiral effective field theory
Thesis for the degree of Doctor of Philosophy
Boris D. Karlsson
Department of Physics
Chalmers University of Technology

Abstract

The scientific method implies a dynamical relationship between experiment and theory. Indeed, experimental results are understood through theories, which themselves are of less value until confronted with experiment. In this thesis I study this relationship by quantifying two key properties of theories: theoretical uncertainties and predictive power.

Specifically I investigate chiral effective field theory (χEFT) and the precision and accuracy by which it reproduces and predicts low-energy nuclear observables. I estimate both statistical and systematic uncertainties. The conclusion is that the latter, which in my approximation originates from omitted higher-order terms in the chiral expansion, are much larger than the former. In relation to this, I investigate the order-by-order convergence up to fourth order in the chiral expansion. I find that predictions generally improve with increasing order, while the additional low-energy constants (LECs) of the interaction makes it more difficult to fully constrain the theory. Furthermore, in order to accurately reproduce properties of heavier nuclei I see indications that it is necessary to include selected experimental data from such systems directly in the fitting of the interaction.

In order to perform these studies I have developed accurate and efficient methods as well as computer codes for the calculation of observables. In particular, the application of automatic differentiation for derivative calculations is shown to be crucial for the minimization procedure. These developments open up new avenues for future studies. For example, it is now possible to do extensive sensitivity analyses of the experimental data and the model; to investigate the power counting from a data perspective; and incorporate more experimental data in the fitting procedure.

Keywords: nuclear physics, χEFT, uncertainty quantification, two-nucleon scattering, few-nucleon physics

Thesis

This thesis consists of an extended summary and the following appended papers. Note that the spelling of the author of this thesis is "B. D. Carlsson" on these papers.

Paper A:
Statistical uncertainties of a chiral interaction at next-to-next-to leading order
A. Ekström, B. D. Carlsson, K. A. Wendt, C. Forssén, M. Hjorth-Jensen, R. Machleidt and S. M. Wild
J. Phys. G 42, 034003 (2015), e-Print: arXiv:1406.6895

Paper B:
Uncertainty analysis and order-by-order optimization of chiral nuclear interactions
B. D. Carlsson, A. Ekström, C. Forssén, D. Fahlin Strömberg, O. Lilja, M. Lindby, B. A. Mattsson and K. A. Wendt
Phys. Rev. X 6, 011019 (2016), e-Print: arXiv:1506.02466

Paper C:
Quantifying statistical uncertainties in ab initio *nuclear physics using Lagrange multipliers*
B. D. Carlsson
Phys. Rev. C 95, 034002 (2017), e-Print: arXiv:1611.03691

Paper D:
Optimization of two- and three-nucleon interactions at N3LO in χEFT
B. D. Carlsson, A. Ekström, C. Forssén
In preparation

Contribution report

My contribution to the papers are listed below.

A. I improved the computer code used for the generation of two-nucleon matrix elements and for fitting the low-energy constants to experimental observables. I participated in discussions about methodology, results and the analysis.

B. I developed several of the methods, performed the optimizations and produced the results. I was involved in the writing of all parts of the paper with the main responsibility for sections II and III.

C. I am the sole author of this paper.

D. I developed several of the methods, performed the optimizations and produced the results. I am involved in the writing of all parts of the paper with the main responsibility for sections II, III and IV.

In addition, the author has been involved in the work leading to the following publications. Note that the spelling of the author of this thesis is "B. D. Carlsson" on these papers. These works are **not** included in this thesis.

Effects of Three-Nucleon Forces and Two-Body Currents on Gamow-Teller Strengths
A. Ekström, G. R. Jansen, K. A. Wendt, G. Hagen, T. Papenbrock, S. Bacca, B. D. Carlsson and D. Gazit
Phys. Rev. Lett. 113, 262504 (2014), e-Print: arXiv:1406.4696

Uncertainty Quantification of the Pion-Nucleon Low-Energy Coupling Constants up to Fourth Order in Chiral Perturbation Theory
K. A. Wendt, B. D. Carlsson and A. Ekström
e-Print: arXiv:1410.0646

Accurate nuclear radii and binding energies from a chiral interaction
A. Ekström, G. R. Jansen, K. A. Wendt, G. Hagen, T. Papenbrock, B. D. Carlsson, C. Forssén, M. Hjorth-Jensen, P. Navrátil and W. Nazarewicz
Phys. Rev. C 91, 051301(R) (2015), e-Print: arXiv:1502.04682

Neutron and weak-charge distributions of the 48Ca nucleus
G. Hagen, A. Ekström, C. Forssén, G. R. Jansen, W. Nazarewicz, T. Papenbrock, K. A. Wendt, S. Bacca, N. Barnea, B. D. Carlsson, C. Drischler, K. Hebeler, M. Hjorth-Jensen, M. Miorelli, G. Orlandini, A. Schwenk, J. Simonis
Nature Phys. 12, 186-190 (2015), e-Print: arXiv:1509.07169

Uncertainty quantification for proton-proton fusion in chiral effective field theory
B. Acharya, B. D. Carlsson, A. Ekström, C. Forssén, L. Platter
Phys. Lett. B 760, 584-589 (2016), e-Print: arXiv:1603.01593

Contents

Acknowledgements

It is thanks to many people that I am able to present this thesis. First I would like to thank my supervisors Christian Forssén, Andreas Ekström and Morten Hjorth-Jensen. I deeply appreciate all fruitful discussions and your patience and understanding. I have also enjoyed many helping and enlightening talks with Håkan Johansson.

I am also grateful to the whole subatomic and plasma physics division at Chalmers, and the research group in theoretical subatomic physics in particular. Many thanks also to the University of Oslo for all hospitality during my PhD studies, and especially to the computational physics group. I also wish to thank the theoretical physics group at Oak Ridge National Laboratory for a rewarding collaboration and interesting discussions.

My thanks goes also to all my friends that have been there for me, and to my family for their support and encouragement.

Finally, I want to thank Malin for your endless love and support.

Part I

Extended summary

Chapter 1

Introduction

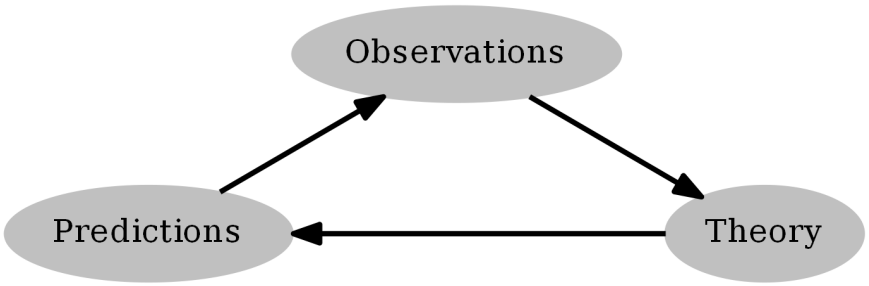

Figure 1.1: The relation between observation and theory. Inspired by observations one can construct general theories explaining the observations. Through predictions the theories can in turn provide guidance for future experiments.

The topic of this thesis is chiral effective field theory (χEFT) and its relation to experimental knowledge. I quantify the precision, accuracy and convergence of χEFT for the description of string interactions between nucleons, and verify the results by comparing the predictions with experimental data. By adopting a unique data perspective, and developing state-of-the-art statistical and computational methods, I have been able to perform new and important investigations of inherent properties of effective field theories. In this introduction I will put my work into a broader context. To this end, I begin in general terms, and gradually zoom in on the relevant physics at the subatomic scale.

Knowledge of the world around us usually begins with observations. In physics research, one task is to understand these through theories and models. From those it is in turn possible to make predictions. It is important to

remember that such descriptions need not be exact, nor able to explain all phenomena around us. They can instead be regarded as simplifications of the world. Theories can be said to aim at finding the underlying reason, or truth, behind the observations. Models on the other hand are used to understand particular phenomena, not necessarily through first principles. To highlight their differences, I will here contrast two particular classes of models and theories encountered in low-energy nuclear physics: phenomenological models and effective field theories. One example of the former is the liquid-drop model [1, 2]. This model explains properties of nuclei by treating them as fluids and the individual nucleons are not resolved. By tuning the parameters of the model to reproduce experimentally known properties, it is possible to provide a gross description of, e.g., how the binding energies of nuclei depend on the number of constituent neutrons and protons. Even though it does not provide a detailed explanation of how nucleons interact, such a rough model is well suited for understanding the broad features of nuclei. To provide more detailed knowledge and to study the behavior of individual nucleons it is necessary to turn to a more microscopic model or theory.

The currently accepted theory that governs the interaction between nucleons is quantum chromo dynamics (QCD) [3]. QCD describes the strong interaction, between quarks and gluons, which in turn are constituents of the nucleons. Although we should in principle be able to describe system of nucleons using QCD directly, using e.g. lattice-QCD, the computational complexity of that approach is so high that it is currently not feasible — even though increasingly sophisticated attempts are being carried out [4–6]. For now, it is necessary to rely on other models and theories to describe the interaction between nucleons.

Already in 1935, before the advent of QCD, Yukawa introduced the concept of pion exchanges for describing the nuclear interaction [7]. Since then, many other models based on meson exchanges have been proposed. One such successful phenomenological model is CD-Bonn [8]. Here, the interaction is modeled as exchanges of various mesons between the nucleons. The coupling strength of the various exchanges are tuned so as to reproduce certain experimental observables. With CD-Bonn it is possible to reproduce, within experimental uncertainties, elastic two-nucleon scattering cross sections up to a laboratory kinetic energy of $T_{\text{lab}} = 350\,\text{MeV}$ as well as bound-state properties of the deuteron. There are also other phenomenological models for the two-nucleon interaction, such as coarse grained delta-shell interactions [9], that are also able to reproduce the above mentioned observables. At first sight it

might look like the issue of the nucleon interaction is solved. However, the phenomenological models lack two crucial properties: predictive power with quantified model uncertainties.

What is predictive power? A possible benefit of a model or theory is its ability to predict results of not yet performed or infeasible experiments. If we trust a model or theory we can use it as a guide for future experiments. Indeed, a model or theory might be *capable* to produce a value for an observable, but do we necessarily *trust* this result? It seems that reliability is at the core of predictive power. For example, many models and theories contain parameters that are tuned in such a way that a set of experimental data are reproduced, as in the examples above. Does such an agreement with experiment necessarily imply an expected agreement outside this set of data? In general, the answer is no. This is particularly not expected for phenomenological models, which usually are constructed with the goal of understanding particular phenomena and only contain partial connection to the underlying theoretical framework. For example, the models mentioned above — CD-Bonn and delta-shell interactions — have no systematic way of including a three-nucleon force, which has been determined to be necessary to describe nuclear observables [10]. It is therefore difficult to determine the accuracy of the model for other types of observables.

This leads to the second shortcoming of phenomenological models; the difficulty of quantifying the uncertainties in the model predictions. Non-zero uncertainties in a prediction does not necessarily make the prediction unusable. To quote George Box [11], (as quoted in reference [12]),

> "Remember that all models are wrong; the practical question is how wrong do they have to be to not be useful."

In other words, uncertainties in the model or theory can be accepted as long as they are known and under control. Uncertainty estimates are crucial not only for experimental results, but for theories and models as well. Disagreements between theoretical predictions and experiments can provide insight into why the model or theory fails to describe the observations only once all of these uncertainties are estimated.

Effective field theories can be employed to avoid the above mentioned shortcomings of phenomenological models. One such theory is χEFT. Knowing the underlying theory, QCD, it is possible to construct a general interaction with pions and nucleons as degrees of freedom that is consistent with the symmetries of QCD [13], in particular the broken chiral symmetry.

It is this connection to QCD that elevates χEFT from being just another model to the status of a theory [14]. The χEFT can be naturally separated into a long-range part, given by pion-exchanges between the nucleons, and an unresolved short-range part of the interaction approximated using contact terms. These are parametrized by a set of low energy constants (LECs), which in practice need to be determined through a fit to experimental data. However, χEFT consists of infinitely many terms, or diagrams. Apart from the practical issue of not being able to calculate all terms, they also involve infinitely many LECs, which cannot all be fitted to a finite set of experimental data. To solution is a power counting scheme, by which the contributions to the interaction can be ordered by their estimated impact at low energies. A calculation at order ν consists of all diagrams that scale as $(Q/\Lambda_\chi)^x$ with $x \leq \nu$. The expansion parameter is the ratio of soft and hard scales in the problem and should preferably be small for the expansion to be effective. Q is the soft scale of χEFT, approximately given by the pion masses ($\sim 140\,\mathrm{MeV}$). By moving to higher orders, the theory is expected to become increasingly precise. This systematic expansion also makes it possible to estimate the theoretical uncertainty from the expected size of the omitted contributions. The power counting scheme and the possibility to estimate uncertainties are precisely the ingredients required to facilitate predictive power.

The main motivation for my thesis work has been to investigate the two important properties — theoretical uncertainties and predictive power — in the specific context of χEFT applied to low-energy nuclear physics. Both of these properties are closely related to the interplay between the theory and the experimental data. The theory predictions with associated uncertainties can be validated only by comparing to experimental results. That is the case also for the predictive power. Furthermore, in the confrontation of χEFT with data, other properties can also be investigated. Model-dependent correlations between different observables can be explored, which makes it possible to determine how dependent an observable is to the values of other observables. Obtained uncertainties and covariances between LECs can tell us something about what data that is needed to constrain the interaction.

This thesis contains an extended summary of the four papers that are described in chapter 6. The outline of the extended summary is as follows: Chapter 2 consists of a more detailed description of χEFT together with the methods that are used to calculate various observables. In chapters 3 I present and analyze the predictions and uncertainties of the chiral interactions fitted at different orders. I take this one step further in

chapter 4 where I study families of interactions to find global relationships and correlations. I present the main conclusions of my work and provide an outlook to future studies in chapter 5.

Chapter 2

From theory to prediction

The purpose of this chapter is to provide a general description of the relevant physics and the methods that have been used in my work to describe the interactions between nucleons. Compared to chapter 1 I here provide a more technical introduction and background to the main work and results presented in this thesis. For more in-depth descriptions, see e.g. reference [14] and paper B. My aim is to outline how to go from the underlying theory of QCD to a theoretical prediction using χEFT.

The first step is to define the general χEFT interaction between pions and nucleons, which is done in section 2.1. In section 2.2 the methods that have been used to calculate theoretical predictions for few-nucleon observables are described. These observables include two-nucleon elastic scattering cross sections as well as bound-state properties of few-nucleon systems. The experimental data that are used in the fitting of the interaction and for comparing predictions are presented in section 2.3, while the methodology for the fitting is described in section 2.4.

2.1 The χEFT framework

In the χEFT employed in my work, nucleons and pions are used as the *effective* degrees of freedom instead of the constituent quarks and gluons. This is a valid approach at low energies, where the nucleons and pions remain stable. χEFT will obey all the symmetries of the underlying theory, QCD, by construction.

Of special interest is the explicitly and spontaneously broken chiral

symmetry [14]. The quark field q entering the QCD Lagrangian can be projected onto a left-handed (q_{left}) and a right-handed (q_{right}) component such that $q = q_{\text{left}} + q_{\text{right}}$. It turns out that if the quarks are massless, the Lagrangian is unchanged by a unitary rotation of either the left-handed or the right-handed component, which is called chiral symmetry. Due to the small (compared to nucleons) but non-vanishing quark masses, chiral symmetry is explicitly broken by QCD. It is still, however, an approximate symmetry and as a consequence one expects to see almost degenerate isospin states and parity states in the hadronic spectrum. This is the case for isospin, e.g. the masses of the neutron and proton are about the same. However, degenerate parity states are not observed in nature [14], implying a spontaneous symmetry breaking. The chiral symmetry breaking along with the other symmetries of the QCD Lagrangian determine, to a large extent, how the pions and nucleons interact at low energy, which is then incorporated into χEFT.

With the symmetries of QCD in mind, one constructs the most general Lagrangian for the interaction between the nucleons and pions [13]. This *effective Lagrangian* will contain an infinite amount of terms, or diagrams, as more and more intermediate states are included. The strengths of most contributions are not fixed by the underlying symmetries. Instead, these contributions are proportional to unknown LECs. This means that the more diagrams we include, the more LECs will have to be determined from data, which in itself is a reduction of the predictive power of the model. For practical calculations to be possible, i.e. without having to include all terms, a *power counting (PC) scheme* is needed, i.e. a way to order the diagrams such that the ones that have the largest impact on the low-energy physics are included first. In this way, it is possible to include the most important diagrams until the desired accuracy is achieved.

The importance of the PC is hard to overstate. If we cannot predict that some diagrams will only have a very small impact on the results, we will have no way to estimate the uncertainty of the model. The ability to estimate the uncertainty of the model is what sets χEFT apart from phenomenological models of the nucleon-nucleon interaction such as meson-exchange models and δ-shell interactions [9]. The PC is also crucial for a correct renormalization. Effective field theories are renormalized order-by-order [14]. This implies that appropriate counterterms need to be included at each order to cancel infinities that arise from the pion-exchange diagrams. One role of the PC is to make sure that the correct counterterms are included

at each order. In my work I have used the standard Weinberg PC [15], although one should note that the topic of PC in χEFT is under some debate [16–18].

When nucleons and pions interact with high relative momentum p, there could be enough energy to create new particles, such as a ρ meson. This can not be predicted by a χEFT where only pions and nucleons are considered. Therefore, the *breakdown scale* Λ_χ of χEFT— i.e. the energy at which the effective-field theory becomes invalid — is around the mass of the ρ meson, $M_\rho \approx 800\,\mathrm{MeV}$. This sets an upper energy scale for our χEFT. On the other hand, the pion masses ($\sim 140\,\mathrm{MeV}$) sets the *characteristic scale* for pion exchanges. The relative momentum p will then be of the order of the pion masses in a low-energy interaction. The PC is then the ordering of the terms in the Lagrangian in powers of Q/Λ_χ, where Q is the *soft scale* given by the pion masses and p, while Λ_χ is the breakdown scale. Each term in the Lagrangian scales according to $(Q/\Lambda_\chi)^\nu$, where ν is the order of the term according to the PC, with $\nu \geq 0$ for all terms allowed by the underlying symmetries [14].

In practice there are more scales involved: the ratio between Q and the nucleon mass, Q/M_N, the mass-difference $(m_u - m_d)/(m_u + m_d)$ of the up and down quarks and the fine-structure constant α which is the expansion parameter for the EM interaction. The nucleon mass gives rise to relativistic corrections and the quark mass difference to isospin breaking effects. All of these scales are combined into an extended PC, allowing an ordering of all contributions. The combination of the scales into a single PC can be done in different ways, in particular the relativistic corrections are sometimes assumed to scale as $Q/M_N \approx (Q/\Lambda_\chi)^2$ [15, 19, 20] and sometimes as $Q/M_N \approx (Q/\Lambda_\chi)$ [14]. In the included papers we employ the first variant, although it is not crucial for the results or the analysis. See paper B for details.

With the PC fixed, the terms, or diagrams, of the strong interaction can be divided into groups, both depending on the order ν and on the type and quantities of the exchanged particles.

The lowest order interaction is leading order (LO), and consists of all $\nu = 0$ terms. There are no terms with $\nu = 1$ due to parity and time-reversal invariance. Therefore the next-to-leading order (NLO) is constructed from all terms with $\nu \leq 2$. From there on it continues with next-to-next-to-leading order (N2LO or NNLO) being $\nu \leq 3$ and N3LO ($\nu \leq 4$).

The diagrams are usually divided into two parts; the contact interaction (V_{ct}), and the pion exchanges where one or more pions are exchanged ($V_{1\pi}$,

$V_{2\pi}$, $V_{3\pi}$, and so on). The pion exchanges constitute the long-range part of the nuclear interactions and are partially determined by chiral symmetry. The contact interaction, on the other hand, is a general parameterization of the short-range physics, with each term proportional to an LEC.

The contact and pion-exchange diagrams entering the interaction at the different orders are shown in figure 2.1. The nucleons and pions are shown with solid and dashed lines, respectively. At LO the leading contact interaction enters, represented by two crossing nucleon lines, together with one-pion exchange (1PE). At NLO there are additional contact interactions and also the leading two-pion exchange (2PE). At N2LO there are corrections to the 2PE and also the leading three-nucleon force appears, consisting of contact interactions and pion exchanges. Finally at N3LO there are many new contributions to the contact interaction and the 2PE. The first four-nucleon diagrams also enter at this order. The three-pion exchange (3PE) appears in both the two-, three- and four-nucleon interactions.

The lowest ν allowed when A nucleons interact is $\nu_A^{(\min)} = 2A - 4$ [14]. Thus, the two-nucleon force enters at LO and the three-nucleon force at NLO. However, at NLO all three-nucleon contributions cancel and the first non-vanishing contribution enters at N2LO [21].

For the calculation of two-nucleon scattering we solve the non-relativistic Lippmann-Schwinger (LS) equation and for the calculation of nucleon bound-state observables we employ the non-relativistic Schrödinger equation. In both cases a *non-relativistic potential* is needed. For details on how this potential is constructed from the effective Lagrangian, see e.g. reference [14].

At N2LO the sub-leading 2PE enters with diagrams proportional to the pion-nucleon LECs c_1, c_3 and c_4. At N3LO the pion-nucleon LECs c_2, $d_1 + d_2$, d_3, d_5 and $d_{14} - d_{15}$ enter.

The 3PE terms entering at N3LO, see figure 2.1, have been shown to be rather small [14] and are therefore ignored.

The contact interaction can be parametrized in different ways. In my calculations I use a partial-wave momentum-basis. A *channel* in this basis is denoted as ${}^{2S+1}L_J$, where S is the total spin, L the orbital angular momentum (with $L = 0, 1, 2$ denoted by S, P, D and so on) and J the total angular momentum. I therefore parameterize each partial wave independently. At a given order, denoted ν_{ct}, only partial waves up to angular momentum $L + L' = \nu_{\text{ct}}$ will have a non-zero contribution, where L (L') is the incoming (outgoing) orbital angular momentum. Thus, the leading-order contact

interaction, $V_{\rm ct}^{\rm (LO)}$, affects only S-waves, proportional to the two-nucleon LECs $\tilde{C}_{^1S_0}$ and $\tilde{C}_{^3S_1}$ The terms from the NLO (N3LO) contact interactions are proportional to the C_x (D_x) two-nucleon LECs. For more details, see e.g. Ref. [14]. For the NLO (N3LO) contact interactions there are 7 (15) two-nucleon LECs needed to parametrize the contact interaction, respectively.

To sum up the LEC dependence at the various orders, all terms are either proportional to or independent of LECs,

$$\begin{aligned}
V_{\rm ct}^{\rm (LO)} &\sim \{\tilde{C}_{^1S_0}, \tilde{C}_{^3S_1}\} \\
V_{\rm ct}^{\rm (NLO)} &\sim \{C_{^1S_0}, C_{^3S_1}, C_{^3S_1-^3D_1}, C_{^3P_0}, C_{^1P_1}, C_{^3P_1}, C_{^3P_2}\}, \\
V_{\rm ct}^{\rm (N3LO)} &\sim \{D_{^1S_0}, \hat{D}_{^1S_0}, D_{^3S_1}, \hat{D}_{^3S_1}, D_{^3S_1-^3D_1}, \hat{D}_{^3S_1-^3D_1}, D_{^3P_0}, D_{^1P_1}, \\
&\qquad D_{^3P_1}, D_{^3P_2}, D_{^3P_2-^3F_2}, D_{^3D_1}, D_{^1D_2}, D_{^3D_2}, D_{^3D_3}\}, \\
V_{1\pi}^{\rm (LO)} &\sim 1, \\
V_{2\pi}^{\rm (NLO)} &\sim 1, \\
V_{2\pi}^{\rm (N2LO)} &\sim \{c_1, c_3, c_4\}, \\
V_{2\pi}^{\rm (N3LO)} &\sim \{1, d_1+d_2, d_3, d_5, d_{14}-d_{15}, c_1^2, c_2^2, c_3^2, c_4^2, c_1c_2, c_1c_3, c_2c_3\},
\end{aligned} \tag{2.1}$$

The various isospin-breaking effects that exist are well described in e.g. Refs. [14, 21]. Most importantly, at NLO there is a splitting of the $\tilde{C}_{^1S_0}$ contact into three different contacts, $\tilde{C}_{^1S_0}^{\rm (pp)}$, $\tilde{C}_{^1S_0}^{\rm (np)}$ and $\tilde{C}_{^1S_0}^{\rm (nn)}$.

The electro-magnetic interaction is the part of the nucleon interaction that only involves the exchange of photons. This is the longest-range part of the interaction. The long-range effects become increasingly important as the energy approaches zero, therefore we include long-range effects at all orders in the chiral expansion. For details, see e.g. paper B.

The three-nucleon interaction, which enters first at N2LO, consists of a 2PE part proportional to the pion-nucleon LECs c_1, c_3 and c_4, a 1PE part proportional to the three-nucleon LEC c_D and a contact interaction proportional to the three-nucleon LEC c_E [22]. c_D and c_E do not appear in the two-nucleon part. At N3LO there are corrections to the N2LO interaction. However, these corrections do not involve any new LECs. The N2LO and N3LO parts of the three-nucleon potential in a momentum-space partial-wave basis are presented in references [22] and [23] respectively.

For a complete N3LO potential the leading four-nucleon interaction is needed, see figure 2.1. The N3LO four-nucleon diagrams consist of four-pion exchanges (4PE), 3PE, 2PE with one two-nucleon contact, and 1PE with two

nucleon-nucleon contacts. Due to the difficulty of including it in many-body calculations, and because it is expected to be small, it is often neglected [14]. This is also what I have done in my work.

One of the advantages of χEFT is that it links two-nucleon physics with pion-nucleon physics. This means that the pion-nucleon interaction can constrain the pion-exchange part of the two-nucleon interaction. The lowest order terms in the pion-nucleon interaction have $\nu = 1$ and do not involve any LECs. At order $\nu = 2$ the pion-nucleon LECs c_1 to c_4 enter. Then $d_1 + d_2$, d_3, d_5 and $d_{14} - d_{15}$ enter at $\nu = 3$ and e_{14} to e_{18} at $\nu = 4$ summing up to a total of 13 pion-nucleon LECs.

At orders LO and NLO in the two-nucleon interaction none of the pion-nucleon LECs enter. At N2LO however, a connection between the two-nucleon and pion-nucleon interactions is established through the pion-nucleon LECs c_1, c_3 and c_4 as these LECs affect both the two-nucleon, three-nucleon and pion-nucleon interactions. For more details regarding the pion-nucleon Lagrangian and the interaction, see e.g. Refs. [24, 25].

When the magnitude of an ingoing or outgoing momentum $\boldsymbol{p}$ approaches the breakdown scale Λ_χ of χEFT, the non-relativistic potential V is no longer accurate and it would cause the LS equation to diverge. Therefore, it is necessary to cut off high momentum contributions in the potential. In the included papers, this is done using a non-local regulator function $f_{\mathrm{NN}}(p)$,

$$V(\boldsymbol{p}', \boldsymbol{p}) \leftarrow\!\shortmid V(\boldsymbol{p}', \boldsymbol{p}) f_{\mathrm{NN}}(p') f_{\mathrm{NN}}(p), \tag{2.2}$$

with

$$f_{\mathrm{NN}}(p) = \exp\left[-\left(\frac{p}{\Lambda}\right)^{2n}\right] \tag{2.3}$$

$$n = 3, \tag{2.4}$$

where Λ is a regulator parameter. In the papers, $n = 3$ is used. The parameter Λ determines at what scattering momentum to cut off the potential. For my purposes, a reasonable upper limit for Λ is the break-down scale $\Lambda_\chi \approx 800\,\mathrm{MeV}$, since it has been argued that no improvements are expected by choosing larger values for Λ [26]. Furthermore, the regulator parameter Λ should not be chosen too low. Experimental two-nucleon scattering observables are evaluated up to energies corresponding to a momentum around $400\,\mathrm{MeV}$ and this value can be considered a lower limit for the regulator parameter.

The three-nucleon force, just like the two-nucleon force, needs to be regulated to cut off unphysical high-momentum states. In our works, this is done using the non-local regulator

$$V \leftarrow V f_{3\mathrm{N}}(p', q') f_{3\mathrm{N}}(p, q), \tag{2.5}$$

where p and q here are the Jacobi momenta and

$$f_{3\mathrm{N}}(p, q) = \exp\left[-\left(\frac{4p^2 + 3q^2}{4\Lambda^2}\right)^n\right], \tag{2.6}$$

where we use the same value $n = 3$ as for the two-nucleon potential.

As stated above, the purpose of the cutoff functions is to remove the high-momentum part of the interaction. However, through correlations between high- and low-momentum states, the predictions for low-energy observables will depend on the cutoff function. To keep the values of these observables cutoff independent, i.e. fixed when changing Λ, the values of the LECs must be refitted in such a way as to keep the low-energy physics unaltered.

2.1.1 Model uncertainty

It is crucial to include the model error when fitting to data. In particular for the data where the experimental uncertainties are smaller than the model error. Otherwise one risks fine tuning, or overfitting, to observables where the model is not expected to yield accurate predictions. Including both the model error and the experimental uncertainty in the fitting procedure also results in more correctly propagated statistical errors, as these should depend on the total uncertainty.

In paper B I developed a method to quantify the model error and include it in the fitting procedure. This method is described below and was later used also in paper D.

At a given order ν, all diagrams up to $(Q/\Lambda_\chi)^\nu$ are included, which means that the impact of the omitted terms should scale as $\mathcal{O}((Q/\Lambda_\chi)^{\nu+1})$. This scaling knowledge still needs to be converted to an actual number, σ_{model}. The experimental data that are used consist mainly of scattering observables and some bound-state properties. Scattering observables are associated with a fixed center-of-mass momentum p. The method used to include model errors is to assume that the real and imaginary parts of each two-nucleon

and pion-nucleon scattering amplitude have an error

$$\sigma^{(\mathrm{amp})}_{\mathrm{model,x}} = C_x \left(\frac{p}{\Lambda_\chi} \right)^{\nu+1} \quad , \quad x \in \{\mathrm{NN}, \pi\mathrm{N}\}, \tag{2.7}$$

where C_{NN} and $C_{\pi\mathrm{N}}$ are scaling constants to be determined. This assumption corresponds to a covariance matrix for the scattering amplitudes of the form $(\sigma^{(\mathrm{amp})}_{\mathrm{model,x}})^2 I$ where I is the unit matrix, and implies that we do not take correlations between the scattering amplitudes into account. In the papers we have made the choice $Q = p$, where p is the scattering momentum, to capture the trend of an increasing model error as the energy increases. Note that the size of the error is the same for each scattering amplitude in this approach. The order of magnitude of the different amplitudes should be similar for this assumption to make sense. The analysis in paper B shows that this is indeed the case for both two-nucleon and pion-nucleon scattering.

For bound-state properties it is not straightforward to determine an energy scale Q, therefore model errors of this type are not estimated for these observables in the included papers.

So far I have discussed the systematic model error due to omitted diagrams. In order to define our two-nucleon potential I introduced regulating functions f_{NN} and $f_{3\mathrm{N}}$, which in my case depend on Λ, the chosen cutoff value. As stated, the values of low-energy observables should not depend on the exact form of $f_{\mathrm{NN,3N}}$ and this is achieved by making the values of LECs depend on the chosen regulator function. However, all regulator-dependence is not removed and as the energy increases this error is expected to increase also. This is another source of systematic model errors which is estimated in e.g. reference [20] by varying the value of the cutoff parameter Λ. In papers B and D we use such an approach to provide a model error estimate for the bound-state properties. I will return to this in chapter 4.

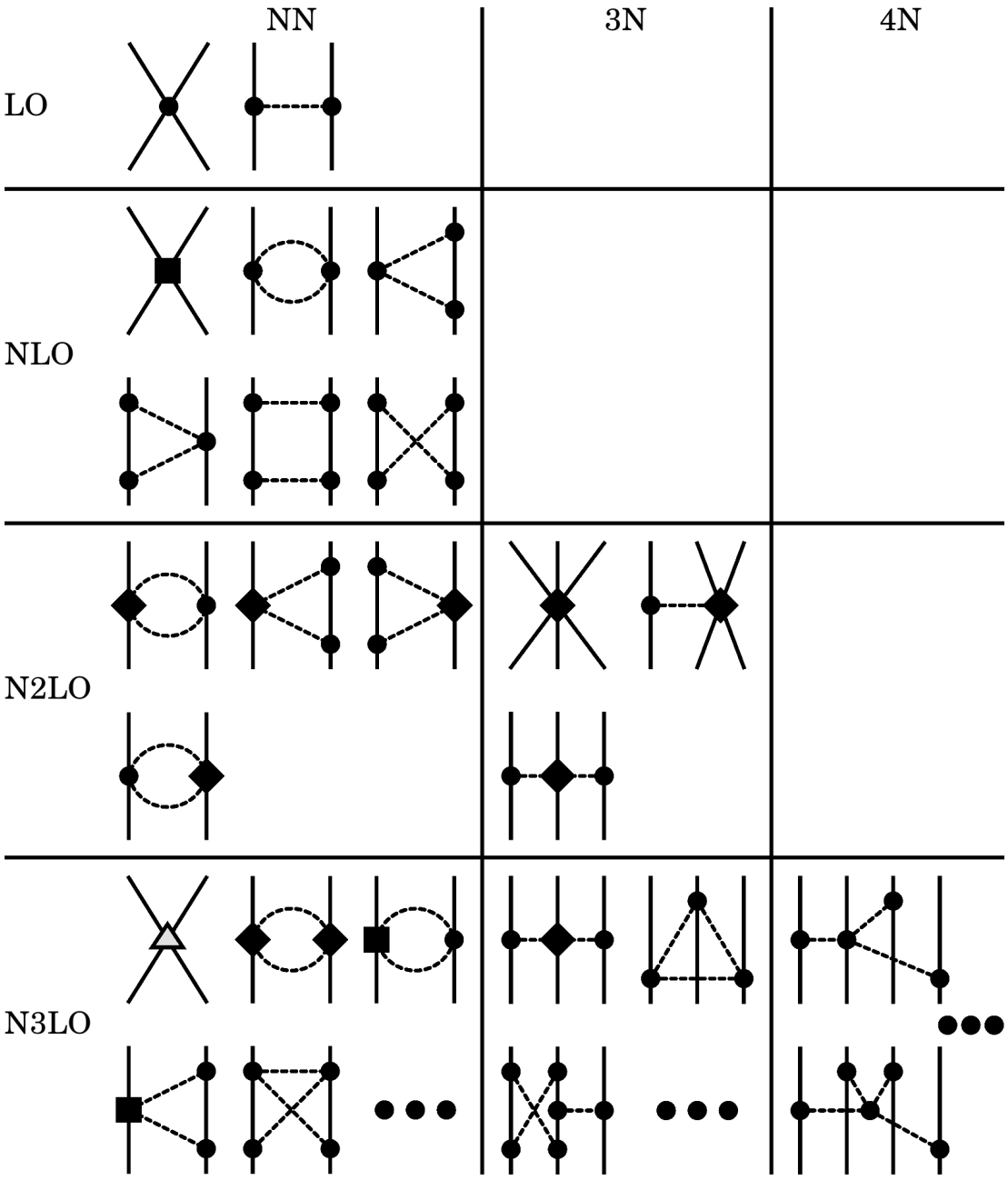

Figure 2.1: Feynman diagrams for the contact and pion-exchange diagrams entering at different orders. Solid (dashed) lines denotes nucleons (pions). A circle, diamond, square and triangle represents a vertex of order $0, 1, 2$ *and* 4 *respectively [14]. Three dots implies that there are more diagrams not shown.*

2.2 Methods of calculation

With the two- and many-nucleon potentials as a starting point, I will here briefly describe the methods used to arrive at predictions for quantities that can be experimentally measured. I will describe methods for calculating cross sections for two-nucleon and pion-nucleon scattering as well as the no-core shell-model (NCSM) for the calculation of bound-state properties of few-nucleon systems. For a more in-depth description of these methods, see paper B.

For the calculation of observables, we use the two-nucleon potential in a partial-wave momentum-basis. Thus, the two-body matrix elements of the form $\langle p'J'L'S'T'T'_z|\,V\,|pJLSTT_z\rangle$ are needed, where p is the relative momentum, J the total angular momentum, L the orbital angular momentum, S the total spin and T (T_z) the total (projected) isospin. Total angular momentum conservation gives $J' = J$. Furthermore, for total spin $S = 0$ and $S = 1$ we have $L = J$ and $|L - J| \leq 1$ respectively. From anti-symmetrization we get $T = 0$ (1) for $L + S$ odd (even). The two-nucleon interaction is isospin conserving, $T = T'$. It is, however, T- and T_z-dependent.

The chiral two-nucleon potential in a momentum basis is given in Refs. [20, 27]. The expressions for the partial-wave decomposition are given in reference [28]. Calculating all necessary matrix elements is a potentially time-consuming task. To make the fittings to experimental data feasible I therefore developed code to make the calculation of matrix elements very efficient.

Two-nucleon elastic scattering observables are calculated from the scattering matrix $M^{s's}_{m'm}(p,\theta,\phi)$ [29, 30], where s (s') and m (m') are initial (final) total spin and spin projection respectively. For a fixed $\boldsymbol{p}$ the M-matrix will be a 4×4 matrix with the basis states $s = 0, m = 0$ and $s = 1, m = -1, 0, 1$. The scattering matrix M satisfies time reversal invariance and parity conservation. Therefore, the M-matrix will be symmetric and only matrix elements with $|L-L'| = 0, 2$ will be non-zero, leaving only six independent quantities. We use the Saclay parametrization of the M-matrix [29] with the complex *amplitudes* a to f to express the observables,

$$\begin{aligned} M(\boldsymbol{q},\boldsymbol{k}) = &\frac{1}{2}\big\{(a+b) + (a-b)(\boldsymbol{\sigma}_1\cdot\widehat{\boldsymbol{q}\times\boldsymbol{k}})(\boldsymbol{\sigma}_2\cdot\widehat{\boldsymbol{q}\times\boldsymbol{k}}) \\ &+ (c+d)(\boldsymbol{\sigma}_1\cdot\hat{\boldsymbol{q}})(\boldsymbol{\sigma}_2\cdot\hat{\boldsymbol{q}}) + (c-d)(\boldsymbol{\sigma}_1\cdot\hat{\boldsymbol{k}})(\boldsymbol{\sigma}_2\cdot\hat{\boldsymbol{k}}) \\ &- e(\boldsymbol{\sigma}_1+\boldsymbol{\sigma}_2)\cdot\widehat{\boldsymbol{q}\times\boldsymbol{k}} - f(\boldsymbol{\sigma}_1-\boldsymbol{\sigma}_2)\cdot\widehat{\boldsymbol{q}\times\boldsymbol{k}}\big\}, \end{aligned} \tag{2.8}$$

where $\boldsymbol{q} \equiv \boldsymbol{p}' - \boldsymbol{p}$ is the momentum transfer and $\boldsymbol{k} \equiv (\boldsymbol{p}' - \boldsymbol{p})/2$ is the average momentum. $\boldsymbol{\sigma}_1$ and $\boldsymbol{\sigma}_2$ are the spin operators for nucleon 1 and 2, respectively. The amplitudes a to f are related to the singlet-triplet representation through linear combinations [30]. For scattering of identical particles, as in proton-proton scattering, the amplitude f will be zero.

Expressions for the different scattering observables as functions of the Saclay parameters can be found in Ref. [29] for identical particles and in Ref. [30] for the more general case of non-identical particles.

For an exact calculation, partial waves for all total angular momenta J from zero to infinity need to be included. In practice it is sufficient to use an upper limit $J_{\max} = 25$ to obtain results that are converged, i.e. the size of the remaining contribution is well below the experimental uncertainty for all experimental data that I have considered.

In addition to nucleon-nucleon scattering I have also calculated pion-nucleon scattering observables. As in the nucleon-nucleon case, these observables are calculated from scattering amplitudes. For a description of how the pion-nucleon amplitudes are constructed, see reference [25] and for a more detailed description of the strong and EM amplitudes see references [31–35].

In addition to scattering observables, I have calculated properties of bound nuclei with $A \leq 4$ in the included papers. The calculated properties are binding energies and radii for ^{2}H (deuteron), ^{3}H (triton), ^{3}He (helion) and the ^{4}He (alpha particle), as well as the quadrupole moment of the deuteron, $Q(^2\mathrm{H})$, and the comparative half-life of triton, $fT_{1/2}(^3\mathrm{H})$.

These observables are calculated using the no-core shell model (NCSM) in a harmonic-oscillator (HO) basis using relative coordinates [36]. The binding energies and wave functions are obtained directly from the eigenvalue problem $\mathcal{H}\,|\Psi_n\rangle = E_n\,|\Psi_n\rangle$, which in a basis representation becomes a matrix eigenvalue problem that is solved using exact diagonalization with the LAPACK library [37].

The HO many-body basis needs to be truncated. In the NCSM this is achieved by an upper limit $N_{\max}$ on the allowed number of HO excitations. For the deuteron, $N^{(2)}_{\max}$ can be chosen high enough that the uncertainty due to a limited model space is much smaller than the experimental uncertainty. For the larger systems, I have employed $N^{(3)}_{\max} = 40$ for three-body calculations and $N^{(4)}_{\max} = 20$ for four-body calculations.

From the obtained wave-functions, the radii, quadrupole moment and comparative half life can be calculated. The comparative half-life of triton is

calculated from [38]

$$\left\langle E_1^A \right\rangle \equiv \left| \left\langle {}^3\mathrm{He} \middle\| E_1^A \middle\| {}^3\mathrm{H} \right\rangle \right|, \tag{2.9}$$

which is the reduced matrix element for the $J = 1$ electric multiple of the axial-vector current.

I have developed routines based on automatic differentiation that enable to extract the derivatives of the observables with respect to the LECs. These derivatives are important in the fitting procedure and to extract accurate statistical uncertainties for the obtained optima.

Starting from an LEC α, the computation of an observable O can be abstracted to a chain of simple mathematical operations,

$$O(\alpha) = f_N(f_{N-1}(\dots f_1(\alpha)\dots)), \tag{2.10}$$

where the functions f_n can be e.g. multiplication with a constant, $f(y) = Ay$; raise to a constant power, $f(y) = y^A$; a trigonometric function, $f(y) = \sin(y)$; or other simple operations implemented in the computer. All of these functions have well-known derivatives. Automatic differentiation relies on the chain rule; given a value $y_n \equiv f_n(\dots f_1(\alpha))$ and its derivative $\partial y_n/\partial\alpha$, one can calculate

$$y_{n+1} \equiv f_{n+1}(y_n) \tag{2.11}$$

$$\frac{\partial y_{n+1}}{\partial \alpha} = \frac{\partial f_{n+1}(y_n)}{\partial y_n} \frac{\partial y_n}{\partial \alpha}. \tag{2.12}$$

Using this equation the desired derivatives can be calculated alongside the values, starting with the LECs all the way to $O(\alpha)$ and $\partial O(\alpha)/\partial\alpha$. In my calculations I need both first- and second-order derivatives of several LECs, which can all be calculated in the same basic fashion as described above.

Another common method for calculating numerical derivatives is finite differences. Two issues with that method are the reliance on the correct estimation of step sizes and the numerical uncertainties due to taking differences of numbers with a very small relative difference. It is particularly difficult to avoid both these problems when both first- and second-order derivatives need to be calculated for several LECs at the same time. This is illustrated in figure B.4, where several derivatives obtained using automatic differentiation and finite differences are compared. The derivatives produced by the latter method sometimes have a large dependence on the step size, with

the optimal step size being different for different derivatives. Derivatives that should be zero are seen to be many magnitudes larger than those obtained by automatic differentiation due to the poor precision of finite differences.

2.3 Experimental data

With the theoretical framework described, I here turn to the experimental side. Measurements of nuclear observables are important to constrain a χEFT description of the nuclear interaction. For this I have used bound-state observables such as binding energies and radii as well as pion-nucleon and nucleon-nucleon elastic scattering observables. The latter can be measured in various settings. It is possible to vary the energy of the impinging nucleons, the type of nucleons, measure the probability of scattering at various angles and to prepare the initial states of the nucleons in polarized states. This has made possible a wealth of different experimental measurements that can be used when comparing or constraining χEFT to experimental values. In my work, I have considered scattering of a proton on either another proton or a neutron. The case of neutron-neutron scattering is difficult to measure experimentally and is therefore not considered.

Experimental scattering observables are usually measured either at several scattering angles or several energies in the same experiment, referred to as a dataset. Due to the large amount of scattering datasets from different experimental groups, there are compilations, or databases, of scattering observables. Two such databases for two-nucleon scattering are the so called SM99 database [39] (see references [8, 40, 41] for more details) used in papers A and B and the so called GR13 database [9, 42, 43] used in paper D. SM99 consists of 4173 measured scattering observables up to laboratory kinetic energy $T_{\text{lab}} = 290\,\text{MeV}$ while the more recent GR13 database includes an increased number of 4753 observables. A benefit of using such databases is that they are "self consistent". This means that flexible models have been used to find a good fit of all considered datasets together with a subsequent statistical analysis to find and remove experimental data points that are not consistent with the other data. Employing such databases is an advantage when fitting χEFT interactions, which are known to have systematic errors at each given order. This is discussed more in section 2.4.

Just as there are databases for two-nucleon scattering, there are databases for pion-nucleon scattering. The database used in our analyses is from the

Washington Institute group [44] and here called WI08. Up to the energy $T_{\text{lab}} = 70\,\text{MeV}$ this database contains 1347 experimentally measured scattering cross sections. The data consists mainly of differential cross sections and some singly-polarized differential cross sections for the processes

$$\pi^{\pm} + p \to \pi^{\pm} + p \quad \text{and}$$
$$\pi^{-} + p \to \pi^{0} + n.$$

Experimental values for the bound-state properties described in section 2.2 together with adopted combined uncertainties from the experiment and the method of calculation are presented in paper B.

2.4 Fitting of low-energy constants

I have described how to construct χEFT nucleon interactions in section 2.1. The general interaction depends on a set of LECs that needs to be determined by finding the "best" agreement with a set of experimental data. In section 2.2 I described how to calculate theoretical values for observables given a set of LECs and in section 2.3 I presented the databases of experimental measurements that have been used in the works I have been involved in. Now I will show how to put these parts together to form a method for the fitting of the LECs to experimental data. This is well described also in papers A and B.

The optimal LECs, i.e. the ones that result in the most accurate reproduction of the experimental values, are determined by minimizing the real-valued objective function

$$\chi^2(\boldsymbol{\alpha}) = \sum_{n=1}^{N} \left(\frac{O_{i,\text{theo.}}(\boldsymbol{\alpha}) - O_{i,\text{exp.}}}{\sigma_{i,\text{total}}} \right)^2 \equiv \sum_{n=1}^{N} r_i^2(\boldsymbol{\alpha}) \tag{2.13}$$

called the chi-squared function. Here, N is the number of experimental values, $O_{i,\text{theo.}}(\boldsymbol{\alpha})$ is the theoretical prediction given the LECs $\boldsymbol{\alpha}$, $O_{i,\text{exp.}}$ is the experimental value, $\sigma_{i,\text{total}}$ is the combined uncertainty in the theoretical and experimental value and r_i are called the residuals.

This is also called non-linear least-squares minimization, and is what has been used in the papers A to D. The name of the function derives from that χ^2 is chi-squared distributed with $N_{\text{dof}} \equiv N - N_{\text{par.}}$ degrees of freedom, where N_{par} is the number of fitted parameters, under the conditions that,

1. The experimental uncertainties are correctly estimated.

2. The experimental values can be treated as normally distributed random variables.

3. The residuals are uncorrelated.

4. The theoretical uncertainties are correctly estimated.

Making sure the first point in the above list is fulfilled is mainly the responsibility of the experimenter. However, as described in section 2.3 it is also possible to compile databases of experimental data where irregular experimental values are removed.

The second and third points are implicitly assumed throughout my analysis, however a few remarks regarding correlated measurements are in order. The experimental values are generally uncorrelated — the measurements do not depend on each other. One important exception is scattering data in the same dataset. For some of these datasets, there is an uncertainty σ_C in the overall scaling of the results given by the experimenter together with the N_d experimental values $O_d^{(\mathrm{exp})}$. The full uncertainty in the experimental results can then be written as

$$(1 \pm \sigma_C)(O_d^{(\mathrm{exp})} \pm \sigma_{d,\mathrm{exp}}), \tag{2.14}$$

where $\sigma_{d,\mathrm{exp}}$ is the experimentally measured statistical uncertainty for that data point. The common, systematic uncertainty σ_C in the results implies that there are correlations between the obtained experimental values, since σ_C is present in each experimental value in a given dataset. To avoid these correlations two steps are taken. First, the model is fitted to the experimental data without including the systematic part. Second, the uncertainty σ_C is accounted for by introducing a fit parameter C, called a normalization constant, which is used to normalize the theoretical predictions. The parameter C is constrained by adding a residual $(C-1)/\sigma_C$ to the chi-squared function. All terms in $\chi^2(\boldsymbol{\alpha})$ for a given dataset are then given by

$$\left(\frac{C-1}{\sigma_C}\right)^2 + \sum_{d=1}^{N_d}\left(\frac{CO_d^{(\mathrm{theo})}(\boldsymbol{\alpha}) - O_d^{(\mathrm{exp})}}{\sigma_{d,\mathrm{total}}}\right)^2, \tag{2.15}$$

For a fixed set of LECs $\boldsymbol{\alpha}$, the value of C is found by minimizing this sum. This can be done analytically, with

$$C = \frac{\frac{1}{\sigma_C^2} + \sum_{d=1}^{N_d} \frac{O_d^{(\mathrm{theo})} O_d^{(\mathrm{exp})}(\boldsymbol{\alpha})}{\sigma_{d,\mathrm{total}}^2}}{\frac{1}{\sigma_C^2} + \sum_{d=1}^{N_d} \frac{\left(O_d^{(\mathrm{theo})}(\boldsymbol{\alpha})\right)^2}{\sigma_{d,\mathrm{total}}^2}}. \tag{2.16}$$

Even though the normalization factors represent a systematic uncertainty in the experiment, the uncertainty σ_C itself is of statistical nature. Therefore, by fitting the normalization constants C this uncertainty can be treated as a statistical uncertainty. Some of the scattering datasets are *floated*, meaning that the value of the constant C is unconstrained experimentally — i.e. $\sigma_C \to \infty$. In these cases, the $(C-1)^2/\sigma_C^2$ term is excluded from equation (2.15) and the corresponding terms in equation (2.16).

The fourth point in the above list, about correctly estimated theoretical uncertainties, has been a central topic of my work and is discussed also in papers B and D. One approach, as done in papers B and D, is to decompose the total uncertainty σ_{total},

$$\sigma_{\mathrm{total}}^2 = \sigma_{\mathrm{exp}}^2 + \sigma_{\mathrm{numerical}}^2 + \sigma_{\mathrm{method}}^2 + \sigma_{\mathrm{model}}^2. \tag{2.17}$$

The experimental uncertainty, σ_{exp}, is the one given by the experimenter. There is also a numerical uncertainty, $\sigma_{\mathrm{numerical}}$, due to the finite precision of computers. In addition, the many-body method used to calculate the theoretical prediction may contain approximations. These are accounted for in σ_{method}. Finally, the uncertainty in the model itself is σ_{model}.

An additional remark regarding correlated residuals is in order here. As both the experimental value and the theoretical prediction is associated with uncertainties, they can both be regarded as random variables. The main difference is that as opposed to the experimental values, the values produced by the model are correlated through the dependence on the LECs. As long as the experimental uncertainty dominates, so that $\sigma_{\mathrm{total}} \approx \sigma_{\mathrm{exp}}$, these correlations are not an issue, as the correlations between the residuals will be negligible. However, if the model uncertainty dominates, so that $\sigma_{\mathrm{total}} \approx \sigma_{\mathrm{model}}$, there can be strong correlations. This is most clearly seen if we assume that we have two experimental measurements of the same observable included in the chi-squared function. Since it is the same observable, the model predictions will be identical and fully correlated, and so also the

residuals. In this case, this results in an over-fitting of this observable, which is not desired. Hence, for residuals with large model uncertainties this is a potential issue with the chi-squared function I have employed.

There are various ways to estimate the numerical values of the model uncertainty. In section 2.1.1 I presented the functional form of the model uncertainty that was used in papers B and D. The general form needs to be complemented with a method for estimating the scale of the uncertainties. One approach is to use the discrepancy between the model and experiment at lower chiral orders as a guide for the next order [45–47]. Another approach, which is what we have used in papers B and D, is to use the obtained discrepancy between the model and experiment from the chi-squared fitting as a guide for the size of the model uncertainty. As stated, a chi-squared value around N_{dof} is expected. A higher value indicates that the total uncertainties in the chi-squared function are estimated to be too low. Assuming the experimental, numerical and method uncertainties are correctly estimated, the too-high value of the chi-squared function is an indication of missing model uncertainty. The values of C_{NN} and $C_{\pi\text{N}}$ introduced in section 2.1.1 are therefore chosen such that the chi-squared per datum for the corresponding scattering data is one. This leads to an iterative process, where a fit of the LECs is performed assuming fixed C_x constants. Once a minimum is found, the values of C_x are updated to correct the chi-squared value. This will slightly alter the location of the minimum, necessitating a new fit. This procedure is repeated until convergence is reached, usually around three iterations. One way to avoid having to deal with model uncertainties is to only include low-energy data in the fitting. Then the model error can be neglected. This is the approach we used in paper A.

The minimization of equation (2.13) is performed using local minimization routines. In paper A we employed POUNDerS [48], which is a derivative-free non-linear least-squares solver. Improved accuracy and speed was achieved in paper B by instead using automatic differentiation to calculate numerically exact derivatives. This enabled us to use e.g. the Levenberg-Marquardt routine [49] to efficiently find a local minimum, which is described in detail in paper B.

Finding suitable starting points for the minimizations is a difficult task. This is further complicated by the fact that the LECs usually are heavily correlated, meaning that the optimal value of each LEC strongly depends on the values of the others. It is therefore advantageous to divide the fitting procedure into smaller steps. One way to do this is to begin with

an optimization against scattering phase shifts. This procedure is described in detail in papers B and D.

Once one or more suitable minima have been found the properties of the model can be studied. This will be discussed in the next two chapters.

Chapter 3

Local analysis

In chapter 2 I outlined how to use χEFT, starting with the broken chiral symmetry of QCD, to construct a well-founded theoretical description of the strong interaction between nucleons. In this chapter I will describe the quality of the resulting fits in section 3.1, along with the obtained model uncertainties and propagated statistical uncertainties in sections 3.2 and 3.3, respectively. I will also briefly determine the benefits of calculating correlations between observables in section 3.4 and of sensitivity analyses in section 3.5. The obtained uncertainties depend on the value and local curvature of the particular minimum under consideration, hence a local analysis. In chapter 4 I will present uncertainties from a global perspective by considering several minima simultaneously.

3.1 Fitting results

The procedure, methods and algorithms used in the fitting procedure are described in section 2.4. Here, I will discuss the resulting minima.

In paper A we constructed an N2LO interaction with the LECs fitted to two-nucleon scattering data with $T_{\text{lab}} \leq 125\,\text{MeV}$. This truncation allowed us to neglect the model uncertainty, see section 2.1.1. The obtained $\chi^2/N_{\text{datum}} = 1.15$ is close to one, which is a further indication that the model uncertainty is small compared to experimental uncertainties. Furthermore, figure A.2 shows fairly normally distributed residuals, which also is an indication of a good fit. The small deviation from a statistically perfect fit is mainly due to the scattering data with $T_{\text{lab}} = 35 - 125\,\text{MeV}$, indicating that the uncertainties

in the model are comparable to experimental uncertainties in this region.

In paper B we presented LO, NLO and N2LO interactions fitted using so-called separate as well as simultaneous approaches. In the separate approach

Table 3.1: Included experimental data for the various nuclear interactions in paper B. Included data types are marked with 'X'. For separate optimizations, the subscript 'i' indicates at what stage the model is optimized to that data. Excluded data-types are indicated with '–'. Effective-range (ER) parameters are used at NLO to constrain the neutron-neutron part of the interaction.

	Scattering data		*nn* ER	bound-state data	
Potential	NN	πN	parameters	^{2}H	^{3}H, ^{3}He
LOsep	X	–	–	–	–
LOsim	X	–	–	X	–
NLOsep	X_1	–	X_2	–	–
NLOsim	X	–	X	X	–
NNLOsep	X_2	X_1	–	–	X_3
NNLOsim	X	X	–	X	X

the pion-nucleon LECs are constrained using only pion-nucleon scattering observables. Once these LECs are fixed, the ones in the two-nucleon sector are fitted to two-nucleon observables and finally the three-nucleon LECs are fitted to three-nucleon observables. See table 3.1 for a more detailed overview. In the simultaneous approach all LECs are fitted to all observable types at the same time. This is a much more demanding approach, which had not been used previously in the field. It was made possible with the help of the efficient framework and algorithms which I helped develop during my thesis work. The simultaneous method is expected to produce interactions with lower total chi-squared values than the separate approach. This is also what we find. In particular, the proton-proton scattering data are much better reproduced using the simultaneous approach. The reason for this is that the pion-nucleon LECs can be tuned to more accurately describe nucleon-nucleon observables. This is achieved without a significantly worse description of the pion-nucleon data. It should also be noted that a clear convergence, in terms of decreasing uncertainties, of the predictions at higher orders is not seen for the interactions fitted using the separate approach, as shown in figure B.9(a).

With the separate approach, there are four minima both at NLO and N2LO. The existence of several minima, i.e. solutions with very different LEC values but similar chi-squared values, is most likely an indication that

the interaction is not constrained well enough by the data used in the fitting. The four minima have an almost identical description of all the scattering data used to fit the LECs. Since we have estimated the model uncertainty for scattering observables, the difference between the minima at the two-nucleon level can be quantified. As I will show below, it turns out that the difference in chi-squared value between the minima are within the variations allowed by the model uncertainty. However, at the two-body level they differ significantly for the $A = 3$ bound-state observables, as seen in table B.III, with only one of them producing reasonable results for those properties. This confirms that more data are needed to obtain a unique solution, which is achieved with a simultaneous fit to both $A = 2$ and $A = 3$ data.

I will now show explicitly that the differences between the obtained interactions are small compared to the estimated model uncertainty. Consider the general quantity

$$\chi^2(X,Y) = \frac{1}{N}\sum_i^N \left(\frac{O_{i,X} - O_{i,Y}}{\sigma^2_{i,\text{model}}} \right)^2 , \tag{3.1}$$

where the sum is over a set of N nucleon-nucleon scattering observables O_i and the predictions from models X and Y are compared and weighted using the estimated model uncertainty $\sigma_{i,\text{model}}$. The size of the model uncertainty for the two minima are quantitatively the same so it is not important which one is used in the sum. Both the method errors and the numerical errors are small compared to the model uncertainty for these observables. It should be noted that in paper B we assume that the model uncertainty scales as $(p/\Lambda)^{\nu+1}$ where p is the scattering momentum, Λ the regulator cut-off parameter and ν is the truncation order in the chiral expansion. As mentioned in that paper, it would be necessary to replace p by the maximum of p and the mass of the pion, m_π, to obtain a correct model uncertainty for the lowest energies. Therefore, I here use only scattering observables with a laboratory scattering energy above 30 MeV when comparing the models. A value of $\chi^2(X,Y)$ less than one is an indication that the difference in the models is small compared to the model uncertainties. All comparisons between the four minima obtained using the separate approach turn out to produce chi-squared values below 0.32 — well below one.

In paper D we applied the simultaneous fitting procedure to the next order, N3LO, using the same data. Each new order increases the flexibility of the interaction, allowing for a more precise description of the experimental

data at the cost of an increasing number of LECs. It is therefore expected that more data are needed when optimizing at this order. Already at N2LO we found that all experimental data included in our simultaneous fitting procedure were needed to find a unique parameterization. It is therefore not surprising that at N3LO the same set of data is insufficient to find a unique solution. Fitting N3LO interactions using the simultaneous approach, we were able to find around a hundred different sets of LECs that produce similar chi-squared values. The conclusion is that even more data need to be included to find a single optimum. In particular, more data to constrain the three-nucleon force would be needed, such as three-nucleon scattering.

So far I have focused on finding the numerical values of the LECs that best describe the experimental data. The next question is how much the model predictions are allowed to vary around these central values while still giving an acceptable fit, i.e. how large are the various uncertainties in the predictions.

3.2 Model uncertainties

In this section I will discuss the estimated model uncertainties in more detail. In section 2.1.1 I presented the functional form of the model uncertainty used in the included papers and in section 2.4 I showed how numerical values can be obtained. This is a simple method for estimating the expected uncertainty of the model as a function of the scattering energy. It is therefore desirable to somehow check the correctness of the approximation. A benefit of fitting the chiral interactions using a chi-squared function is that normally distributed residuals are expected, as stated in section 2.4. If this is not fulfilled it could be due to an incorrectly estimated model uncertainty. Thus, a comparison to experimental data is necessary both for obtaining the central values of the LECs as well as for quantifying these uncertainties in the model. Other methods for estimating this uncertainty will be demonstrated in chapter 4.

In paper B we analyzed the quality of the estimated model uncertainty for scattering observables in various ways. Figure B.3 highlights that the Saclay amplitudes indeed are of comparable sizes. This is important since the uncertainties introduced to the amplitude are absolute quantities. In figure B.9 we showed the resulting model uncertainties for some selected scattering observables. The simultaneously optimized potentials have the expected behaviors of larger uncertainty with higher kinetic energy and decreasing

uncertainties with increasing order. This is a promising result hinting at a convergence of χEFT. Still, there are indications that the estimate of the model uncertainty has deficiencies and two comments are in order. First, the small deviations from normality of the residuals shown in figure B.2 is explained to be due to the model uncertainty. In particular, the high excess kurtosis is an indication that there are too many small residual values, i.e. the residual distribution is strongly peaked at zero. Second, in figure B.10(a) we show the estimated scale of the model uncertainty when fitting to different amounts of scattering data. The fact that a larger model uncertainty is needed when only low-energy data are included indicates that the model uncertainty for the predicted high-energy data is estimated to be too large.

I will now check the correctness of the energy scaling of the model uncertainty by examining the distribution of residuals in more detail. If the sizes of the residuals have a non-constant dependence on the scattering energy p this is an indication that the scaling may need to be modified. This dependence for the two-nucleon scattering data using the simultaneously optimized N2LOsim potential from paper B with $\Lambda = 500\,\mathrm{MeV}$ and $T_{\mathrm{lab}}^{\mathrm{max}} = 290\,\mathrm{MeV}$ as a function of the laboratory scattering energy is visualized in figure 3.1. The average values of the residuals are closer to zero for larger energies, indicating a slight overestimation of the model uncertainty. For comparison, average residual values when not including the model uncertainty are also shown. This tells us two things. First, above $T_{\mathrm{lab}} \approx 125\,\mathrm{MeV}$ the model uncertainty starts to dominate over the experimental uncertainties. This justifies the use of scattering data only up to this energy in paper A where the model uncertainty was not included in the fitting procedure. Second, despite that the simple form of the model uncertainty introduced in section 2.1.1 and employed in papers B and D is not completely correct, it is a large improvement over not using any model uncertainty. The conclusion is that this form qualitatively captures the size of the model uncertainty. With the aid of the various statistical tools presented here and in paper B, improved functional forms for the model uncertainty may be found.

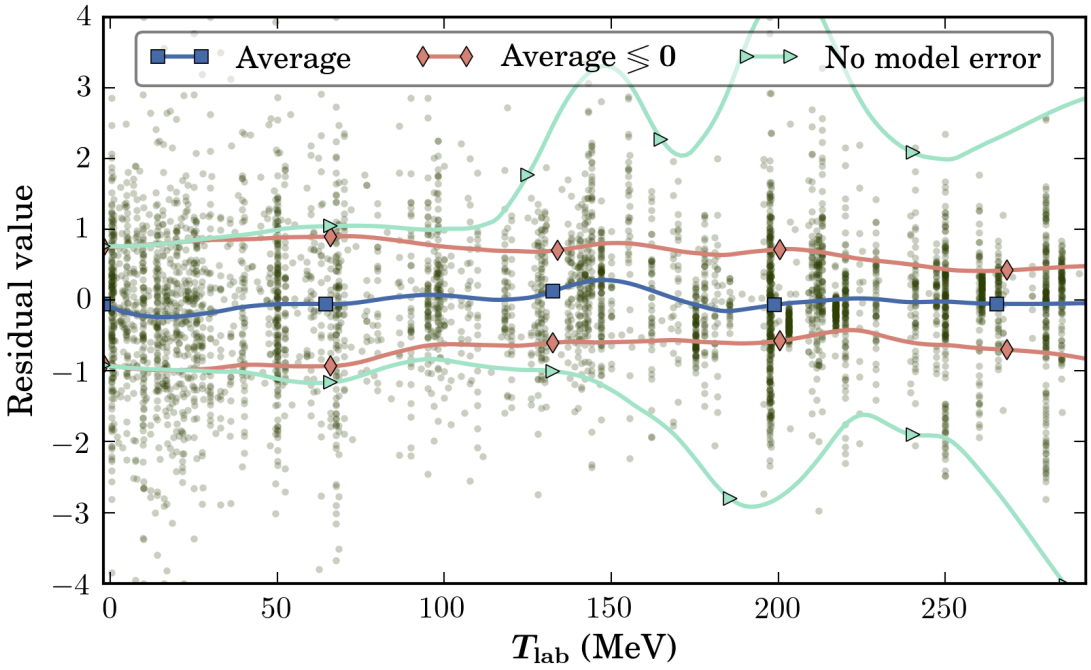

Figure 3.1: Green circles: obtained two-nucleon scattering residuals for the N2LOsim potential from paper B with $\Lambda = 500\,\mathrm{MeV}$ *and* $T_{\mathrm{lab}}^{\mathrm{max}} = 290\,\mathrm{MeV}$ *as a function of the laboratory scattering energy. Blue line with squares: a moving average of the residual values. Red line with diamonds: a moving average of only the positive and negative residuals separately. The distance between the red lines decrease with increased energy, indicating that the uncertainty for large energies is estimated to be too large. As a comparison, the teal line with triangles shows average positive and negative residual values when not including the model uncertainty. In that case the residuals are much larger, demonstrating the importance of the model uncertainty.*

3.3 Statistical uncertainties

Statistical fluctuations of experimental results give rise to statistical uncertainties in the theoretical predictions. These uncertainties together with the accompanying statistical analyses is a central topic in my work. In this section I will briefly describe and derive the basic equations I have used.

The fitted LECs can be treated as random variables, just as the residuals in equation (2.13). The variances and covariances of the LECs are obtained by studying the increase of the chi-squared value around the minimum $\boldsymbol{\alpha}_0$ as a function of the LEC values $\boldsymbol{\alpha}$, $\chi^2(\boldsymbol{\alpha}) - \chi^2(\boldsymbol{\alpha}_0)$. The first non-vanishing term in the Taylor-expansion of this quantity will be the quadratic terms, i.e.,

$$\chi^2(\boldsymbol{\alpha}) - \chi^2(\boldsymbol{\alpha}_0) \approx \frac{1}{2}\Delta\boldsymbol{\alpha}^T H \Delta\boldsymbol{\alpha}, \tag{3.2}$$

where H is the Hessian matrix of χ^2 with respect to the LECs at the minimum $\boldsymbol{\alpha}_0$ and $\Delta\boldsymbol{\alpha} \equiv \boldsymbol{\alpha} - \boldsymbol{\alpha}_0$. Assuming the approximation is valid, this expression is chi-squared distributed with $N_{\boldsymbol{\alpha}}$ degrees of freedom [50]. Consider now the *rotated* LECs, defined from the eigenvalue decomposition of H, $H = UDU^T$, where U is a unitary matrix with the eigenvectors of H as column vectors and D is a diagonal matrix with the eigenvalues of H on the diagonal. In the minimum the Hessian matrix is positive definite, which guarantees that this decomposition exists. From this, the rotated LEC vector is defined as $\boldsymbol{x} = U^T\Delta\boldsymbol{\alpha}$. The increase in chi-squared value can then be written as

$$\frac{1}{2}\boldsymbol{x}^T D \boldsymbol{x} = \frac{1}{2}\sum_{n=1}^{N_{\boldsymbol{\alpha}}} x_i^2 D_{ii}. \tag{3.3}$$

Since this is chi-squared distributed, each x will be normally distributed with variance $2/D_{ii}$. The covariance matrix C of the original LEC vector will then be

$$C \equiv \mathrm{Cov}(\boldsymbol{\alpha}_0) = 2UD^{-1}U^T = 2H^{-1}. \tag{3.4}$$

The expected value of $\chi^2(\boldsymbol{\alpha}_0)$ is N_{dof}. If the model does not agree well with the data, a larger value could be obtained. In such cases the statistical uncertainties will be underestimated. To correct this, a simple procedure is to scale all uncertainties entering equation (2.13) with a so called Birge factor [51] equal to $\sqrt{\chi^2(\boldsymbol{\alpha}_0)/N_{\mathrm{dof}}}$. Increasing the uncertainties in the residuals will increase the statistical uncertainties in the LECs, thus

compensating for the discrepancy between model and experiment. With a Birge factor the covariance matrix C will be $\mathrm{Cov}(\boldsymbol{\alpha}_0) = 2\chi^2(\boldsymbol{\alpha}_0)N_{\mathrm{dof}}^{-1}H^{-1}$.

In the above derivation, I assumed that the chi-squared surface around the minimum is quadratic. In paper D we found, through direct evaluations of the chi-squared function around the minima, that the obtained surfaces are not quadratic in all directions as a function of the LECs. Instead they display a fourth-order dependence. To correctly estimate statistical uncertainties in these cases other methods should be used. One possibility is to use the Lagrange multiplier method, which makes no assumptions on the shape of the chi-squared surface. This method is explained and demonstrated in paper C. In that paper, I compare obtained statistical uncertainties using both the Lagrange multiplier method and the above mentioned method based on the covariance matrix of the LECs. I found that when the quadratic approximation in equation (3.2) is valid, these methods agree. When the approximation does not hold, the Lagrange multiplier method results in more correct uncertainties as this method does not assume a quadratic chi-squared surface.

In my fits up to N2LO the chi-squared surfaces are quadratic and the covariance matrix for the LECs can be used to propagate statistical uncertainties to the theoretical predictions. The LECs are assumed to be distributed according to a multi-variate normal distribution given by $\mathrm{Cov}(\boldsymbol{\alpha}_0)$. A straightforward method to obtain statistical uncertainties for model predictions is to draw N sample points from this distribution, calculate the model prediction for each sample point and obtain the uncertainty from the resulting spread of values. The disadvantage of this brute-force approach is the computational requirements when N is large. For a more efficient calculation, the value of an observable O around the central value $O_0 \equiv O(\boldsymbol{\alpha}_0)$ can be estimated using either a first- or second-order Taylor expansion. This approximate expression for O can either be used to evaluate the values at the sample points or inserted into an explicit formula for the variance,

$$\mathbb{E}[O] = O_0 + \frac{1}{2}\,\mathrm{tr}\,(Ch_0) \tag{3.5}$$

$$\sigma_O^2 = j_0^T C j_0 + \frac{1}{2}\,\mathrm{tr}\left((Ch_0)^2\right), \tag{3.6}$$

where $\mathbb{E}[O]$ is the expectation value of O and j_0 (h_0) is the Jacobian (Hessian) of O at the point $\boldsymbol{\alpha}_0$. See paper C for more details.

Once the statistical uncertainties have been estimated, one can ask how large they are, compared to other sources of uncertainties such as the

uncertainty in the model itself. For the chiral interactions studied in paper B we conclude that systematic uncertainties from the model are generally much larger than the statistical uncertainties for scattering data, indicating that the latter can be ignored. However, even though the statistical uncertainties are small, they can provide useful insights. They can be used to calculate correlations between observables and performing sensitivity analyses. This will be discussed in the next two sections.

3.4 Correlations

Statistical correlations measure the relationship, if any, between different quantities. For example, the average outside temperature on the earth is correlated with the latitude, with higher temperatures closer to the equator. However, the temperature is much less correlated with the longitude. There exist different methods for measuring correlation. The Pearson linear correlation coefficient is a quantity that is commonly used and is also the type of correlation I will focus on here. It measures the amount of linear dependence between two random variables X and Y. It is defined directly from the variances and covariance of the two quantities,

$$\mathrm{Corr}(X,Y) \equiv \frac{\mathrm{Cov}(X,Y)}{\sqrt{\mathrm{Cov}(X,X)\,\mathrm{Cov}(Y,Y)}}. \tag{3.7}$$

With this definition, $-1 \leq \mathrm{Corr}(X,Y) \leq 1$. A value of $+1$ signifies an exact linear dependence where an increase in X always means an increase in Y, while for -1 an increase in X means a decrease in Y. It is important to note that this quantity only measures the linear dependence between X and Y. In paper B we noted that, with the separate minimization scheme, we obtained large statistical uncertainties that resulted in a non-linear dependence between observables. Such dependencies are not accurately captured by the Pearson linear correlation coefficient. With the simultaneous minimization scheme the statistical uncertainties are small and the dependence between variables was found to be linear. The covariance between two observables is obtained in the same fashion as their variances, described in section 3.3,

$$\mathrm{Cov}(X,Y) = j_X^T C j_Y + \frac{1}{2}\,\mathrm{tr}\left(C h_X C h_Y\right), \tag{3.8}$$

where C is the covariance matrix for the LECs, and $j_{X,Y}$ and $h_{X,Y}$ denotes the Jacobian and Hessian of observable X and Y with respect to the LECs at the minimum $\boldsymbol{\alpha}_0$.

When fitting the chiral interactions, it is important to constrain all directions in the space of LECs. It is therefore desirable to include observables that are uncorrelated in the fitting process, since this means they constrain different directions. For example, the deuteron binding energy has very small experimental, method and numerical uncertainties. Including other observables with larger uncertainties that correlate strongly with the deuteron binding energy is therefore not expected to improve the model much. On the other hand, an observable that is difficult to compute theoretically can be replaced by an "easier" observable to the same effect, if they are strongly correlated. However, correlations between observables are local properties, meaning that the correlations can in principle be different for different minima. I will discuss global trends and correlations in section 4.2.

As an example of how obtained correlations can be used to gain insights into the model, I will study the neutron-proton total elastic scattering cross section as a function of the laboratory kinetic energy, $\sigma_{\text{np}}^{\text{tot}}(T_{\text{lab}})$. In papers B and D we presented results for the values and model uncertainties of this quantity up to order N3LO. Here I will instead study the statistical correlations between the cross section at different energies, denoted $\text{Corr}(T_{\text{lab},1}, T_{\text{lab},2})$ for the correlation at kinetic energies $T_{\text{lab},1}$ and $T_{\text{lab},2}$. The goal of this is to investigate the size of the correlations as a function of the difference in scattering energy. χEFT is a low-energy expansion, with higher orders primarily correcting the high-energy physics. Therefore, LECs entering at different orders should have their primary impact at different energies. One way to check this assumption is with the aid of correlations. It would be expected that the correlation between two scattering observables with a large energy difference should have a low correlation, indicating that different LECs affect the two cross sections. Note that I here focus on the LECs directly. One can also ask the question of whether the low-energy observables are sensitive to high-energy features of the interaction. This is done in e.g. reference [52], with the conclusion that there exists a decoupling between low- and high-energy regions.

The squared correlations, $\text{Corr}^2(T_{\text{lab},1}, T_{\text{lab},2})$, for an N3LOsim potential, is shown in figure 3.2. The expected trend of weaker correlations with larger differences in energies is clearly seen. To study this more systematically, I

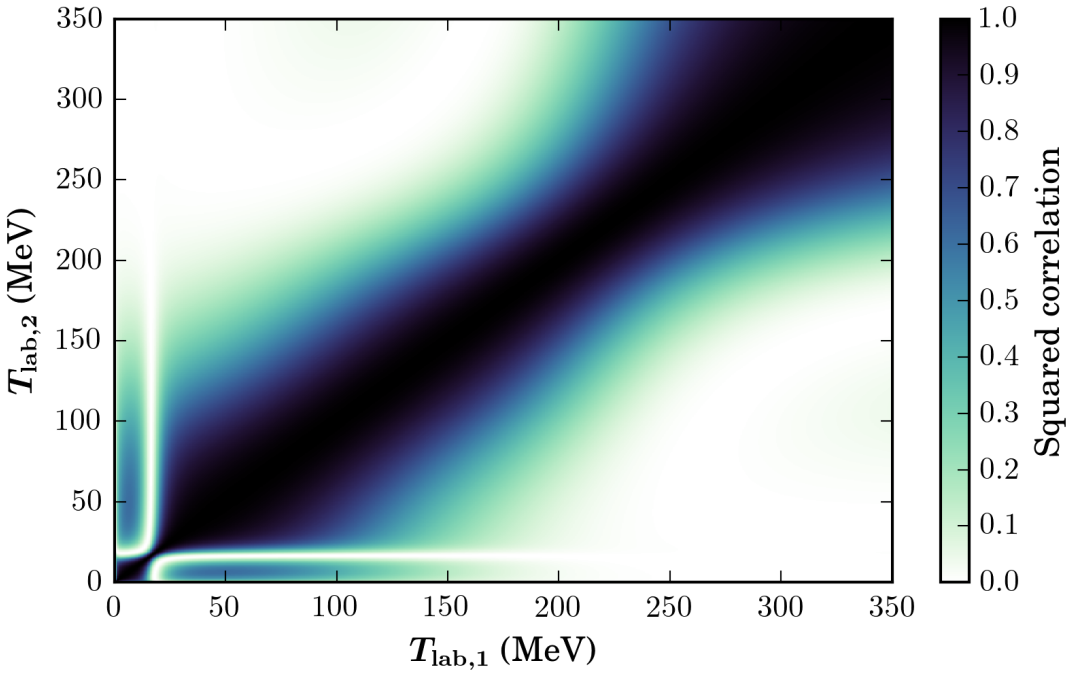

Figure 3.2: Correlation matrix for the neutron-proton total elastic scattering cross section as a function of the laboratory kinetic energy for the N3LOsim potential with $\Lambda = 500\,\mathrm{MeV}$ *and* $T_{\mathrm{lab}}^{\mathrm{max}} = 290\,\mathrm{MeV}$*. Shown as a gradient is the correlation squared, with darker tones signifying stronger correlations. Moving away from the diagonal, i.e. with larger energy differences, a trend of decreasing correlation is seen, indicating a "decoupling" of the energy scales. The correlation matrices for the other N3LOsim potentials show a similar behavior.*

construct an *auto-correlation* function,

$$a^2(\Delta T_{\mathrm{lab}}) = \frac{\int_{\Delta T_{\mathrm{lab}}}^{\max(T_{\mathrm{lab}})} w(T)\,\mathrm{Corr}^2(T - \Delta T_{\mathrm{lab}}, T)\,\mathrm{d}T}{\int_{\Delta T_{\mathrm{lab}}}^{T_{\mathrm{lab,max}}} w(T)\,\mathrm{d}T} \tag{3.9}$$

where w is a weighting factor. I will use $w(T) = 1$ for simplicity and for the integration I use $\max(T_{\mathrm{lab}}) = 350\,\mathrm{MeV}$. The function a is the squared average correlation along the diagonals of the correlation matrix. It estimates the average correlation between scattering observables at an energy difference of ΔT_{lab}.

It is instructive to compare the autocorrelation function a for different orders. This is done in figure 3.3. For the LO potential the correlation is close to 1 for all energy differences. This is not surprising as there are only

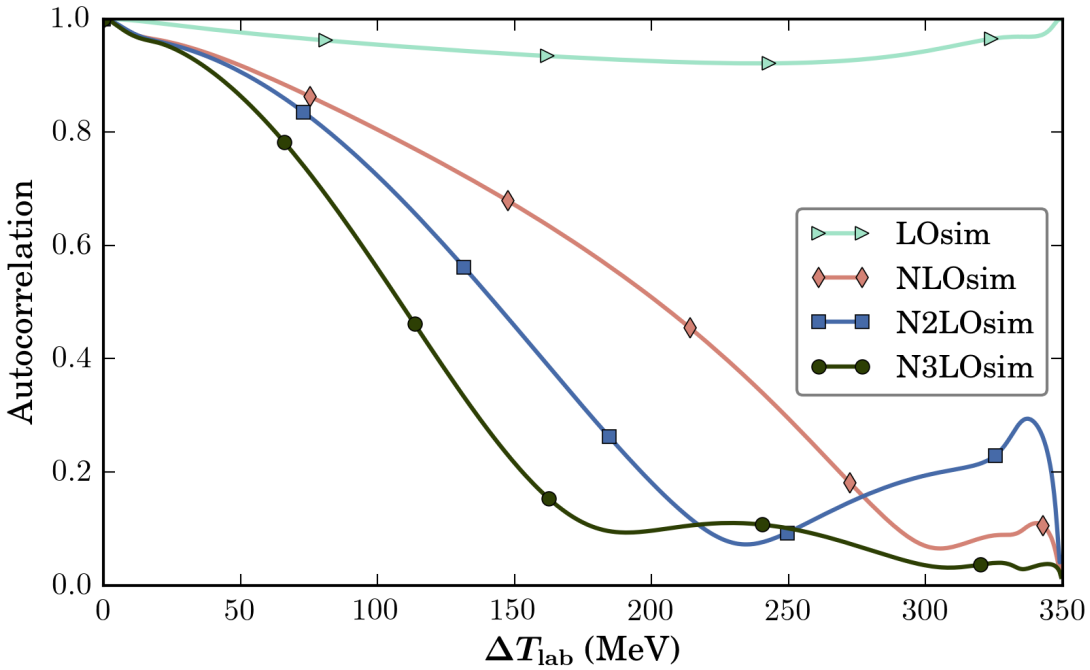

Figure 3.3: Autocorrelation function a for the neutron-proton total elastic scattering cross section as a function of the laboratory kinetic energy for the NxLOsim potentials with $\Lambda = 500\,\mathrm{MeV}$ *and* $T_{\mathrm{lab}}^{\mathrm{max}} = 290\,\mathrm{MeV}$*. The correlation is seen to generally decrease with increased energy difference and decreases faster for higher orders.*

two LECs at this order. These LECs thus determine the cross section at all energies, and the values will then be highly correlated. At each new order, more LECs are added that determine increasingly higher-energy physics. The result is that different energies are determined by different LECs, making the correlations weaker. In the next section I will look at methods to determine which energies that are sensitive to which LECs.

3.5 Sensitivity analysis

A sensitivity analysis tries to answer the question of how sensitive the model predictions are to variations in the model parameters. It is also possible to turn this question around and ask how sensitive the model parameters are to changes in the data used to constrain the model. I will here present these two ways of performing a sensitivity analysis.

I will here start with the second method and gauge the amount of change in the LECs when the value of one or more fit observables are slightly perturbed. Let the experimental value of a single observable in the chi-squared function (c.f. equation (2.13)) be slightly perturbed,

$$O_{i,\text{exp}} \to O_{i,\text{exp}} + \Delta O_i. \tag{3.10}$$

The modified chi-squared function will then be

$$\chi^2_{\text{mod.}}(\boldsymbol{\alpha}) = \chi^2(\boldsymbol{\alpha}) - 2r_i(\boldsymbol{\alpha})\Delta r_i + (\Delta r_i)^2, \tag{3.11}$$

where $\Delta r_i \equiv \Delta O_i/\sigma_i$. The last term in the equation is independent of the LECS and can therefore be ignored. The question is how much do the LECs change when fitting to $\chi^2_{\text{mod.}}$. Already here it is interesting to note the similarities between this modified chi-squared function and the Lagrange multiplier-equation $f(\boldsymbol{\alpha}, O, \lambda)$ defined in equation (17) in paper C. Apart from irrelevant constants, and with $\lambda = -2\Delta r_i/\sigma_i$, it is the same equation. We can therefore immediately arrive at the desired expression for the approximate change in the LECs,

$$\frac{\Delta\boldsymbol{\alpha}}{\Delta r_i} = 2\left(H - 2h_{r,i}\Delta r_i\right)^{-1} j_{r,i}, \tag{3.12}$$

where $j_{r,i}$ and $h_{r,i}$ are the Jacobian and Hessian of the residual r_i and H is the Hessian matrix of χ^2, all with respect to the LECs at the minimum $\boldsymbol{\alpha}_0$ of the original chi-squared function. Now, let $\Delta r_i \to 0$ and use that the covariance matrix $C = 2H^{-1}$ (assuming H has already been scaled with the Birge factor [51]), the equation becomes

$$\frac{\partial\boldsymbol{\alpha}}{\partial r_i} = C j_{r,i}. \tag{3.13}$$

This is the the same equation as for the sensitivity matrix presented in reference [12], if $j_{r,i}$ is extended to a matrix, J_r with one column for each residual. Note also that although I initially assumed that the residual is included in the original chi-squared function, it is evident from the correspondence to the Lagrange multiplier equation that this must not be the case since the latter equation is valid for any observable. This means that the sensitivity of the model to new observables can be probed.

Equation (3.13) can be used in several different ways. The residuals of the chi-square function can be divided into groups. The sensitivity vector $\boldsymbol{S}$,

measuring the sensitivity of the LECs to a global change of the residuals in group M_n, is then

$$\boldsymbol{S}(M_n) = C \sum_{i \in M_n} j_{r,i}. \tag{3.14}$$

The grouping can be done e.g. by observable type or by energy scale. Note that this sum can induce cancellations between residuals. This is beneficial when probing the model response to a change in a group of observables included in the chi-squared function. If one is more interested in the average sensitivity of LECs to certain groups of data, an averaging of the absolute values of the Jacobians can be used instead.

One potential pitfall is that LECs can be sensitive to observables both directly but also through correlations. For example, a change in one observable might cause a direct change in LEC a. However, that change in a necessitates a change in b to correct other parts of the model. That is, sensitivity arises both from the diagonal and the off-diagonal elements of the covariance matrix C. If one wants to measure only direct sensitivity, or sensitivity within groups of LECs without correlations between the groups, this is possible by assuming from the start that all other LECs are fixed. This will result in a reduced Hessian H_{red}, which then results in a reduced correlation matrix C_{red}.

There are many other ways in which equations (3.12) and (3.13) can be used. For example, from the obtained $\Delta\boldsymbol{\alpha}$ one can probe the impact on the values of the LECs with the quantity [12]

$$\sqrt{\sum_i \frac{(\Delta\alpha_i)^2}{C_{ii}}}. \tag{3.15}$$

This measures how much the LECs change in relation to their statistical uncertainties. One could also use the change in the original chi-squared function as a measure, to also include correlations,

$$\Delta\chi^2 = \frac{1}{2}(\Delta\boldsymbol{\alpha})^T H \Delta\boldsymbol{\alpha}. \tag{3.16}$$

This measures how sensitive the chi-squared value is to a change in the value of the residual r_i.

With the aid of the sensitivity measure $\boldsymbol{S}$, defined in equation (3.14), I will now investigate the sensitivity of groups of observables included in the

fitting of the N3LOsim potential with $\Lambda = 500\,\text{MeV}$ and $T_{\text{lab}}^{\text{max}} = 290\,\text{MeV}$. I divide all experimental data into the four groups: neutron-proton scattering, proton-proton scattering, pion-nucleon scattering, and properties of bound nuclei. For each LEC α I calculate the relative sensitivities $\zeta(\alpha, M_n)$ for the groups of observables,

$$\zeta(\alpha, M_n) \equiv \frac{|S_\alpha(M_n)|}{\sum_{j=1}^{4} |S_\alpha(M_j)|}. \tag{3.17}$$

The result is presented in figure 3.4. The two-nucleon contact LECs have

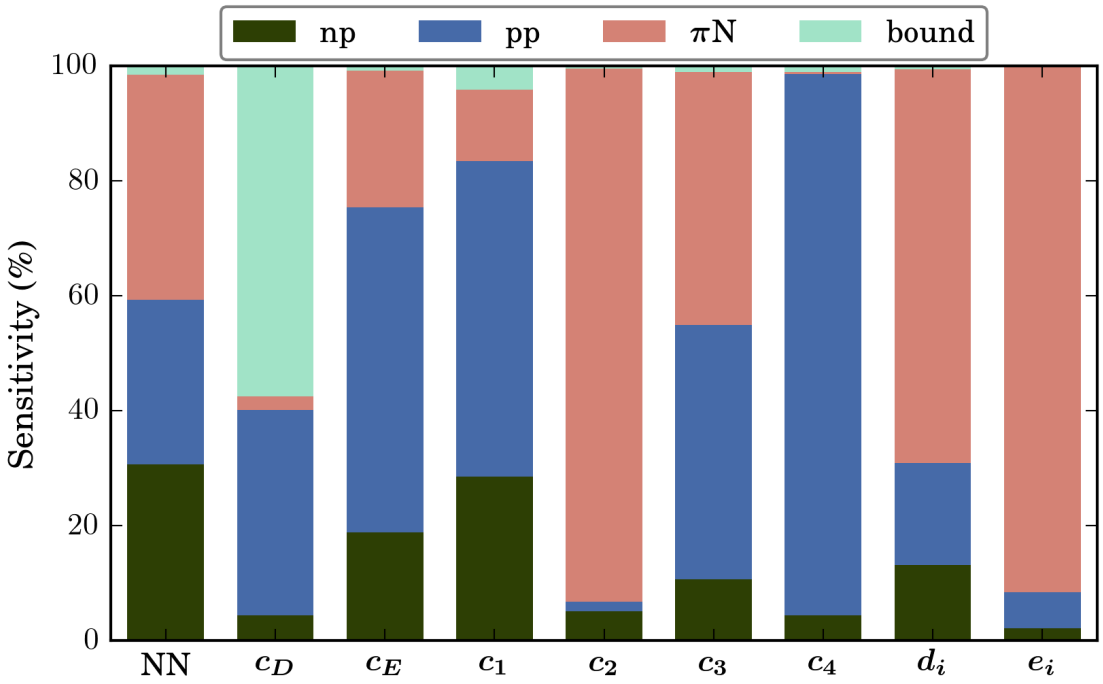

Figure 3.4: For each LEC or group of LECs on the x-axis, the relative sensitivities $\zeta(\alpha, M_n)$ (c.f. equation (3.17)) of the LEC values to a global change in the values of the residuals in four groups of observables are presented along the y-axis. The three first groups are two-body scattering observables for neutron-proton, proton-proton and pion-nucleon scattering respectively. The last group consists of the bound-state properties. NN signifies an average of all the two-nucleon contact interaction LECs, while d_i and e_i are averages of the corresponding pion-nucleon LECs.

been averaged together in one column, since their sensitivities are similar. The same is true for the pion-nucleon d_i and e_i LECs. There are many interesting aspects of this figure: For the two-nucleon contact LECs the

sensitivity is well spread out. There are only eight observables for the bound states, whereas there are thousands of scattering observables, making the sensitivity to the bound-state observables relatively large. Note that the sensitivity of the two-nucleon contact LECs to the pion-nucleon data arises through correlations. The three-nucleon LECs c_D and c_E have a direct effect only on bound-state observables. Despite this, the value of c_E is most sensitive to a global change in the pp scattering data. This highlights the necessity to perform a simultaneous fit of all LECs. In contrast, c_D is sensitive mainly to the triton half life. It is not surprising that the e_i are mainly sensitive to the pion-nucleon scattering data, as these LECs enter only in the pion-nucleon scattering amplitudes. The d_i, which enters first at N3LO in the two-nucleon scattering amplitude, mainly affects the pion-nucleon scattering also. The c_i vary more in their sensitivities; c_1 and c_3 enter at N2LO and affect mainly the central part of the potential; c_4 also enters at N2LO in the isospin-dependent part of the potential, affecting mainly the tensor and spin parts of the potential; c_2 enters the two-nucleon interaction first at N3LO leading to a weaker impact on the two-nucleon scattering observables. The high relative sensitivity of c_4 to the proton-proton scattering data is mainly due to low sensitivities to other types of data. This, in turn, is due to large cancellations in the sum in (3.14) for these types of data. Overall the pion-nucleon scattering has a large influence, despite that the experimental uncertainties generally are large. This indicates that more precise measurements of pion-nucleon scattering cross sections could have a large impact on the two-nucleon interaction.

The other method for probing sensitivities that I want to introduce can be used to study the obtained statistical uncertainties directly. If we, for a moment, ignore correlations, the linear expression for the statistical variance of an observable O can be written as

$$\sigma_O^2 = \sum_{i=1}^{N_{\boldsymbol{\alpha}}} \left(\frac{\partial O(\boldsymbol{\alpha})}{\partial \alpha_i} \right)^2 C_{ii} \equiv \sum_{i=1}^{N_{\boldsymbol{\alpha}}} \sigma_{O,i}^2. \tag{3.18}$$

Here it is evident that the statistical variance of the observable can be decomposed into contributions from individual LECs or groups of LECs. Strictly speaking, with a non-linear expression for the statistical uncertainty such as equation (3.6), together with strong correlations, equation (3.18) is not valid. However, it is still desirable to define a partial variance due to a subset $\mathbb{G}_m$ of the LECs. To define the partial variances, consider an obtained minimum with LECs $\boldsymbol{\alpha}$ and assume that only the LECs in $\mathbb{G}_m$ are allowed

to vary. The other LECs remain fixed at the values at the minimum. The variance of O obtained from only these variations is denoted $\sigma^2_{O,\mathbb{G}_m}$ and is the definition of the partial variance. Dividing the LECs into M groups, I define the normalized partial variance for group $\mathbb{G}_m$ as

$$\eta(\mathbb{G}_m) \equiv \frac{\sigma^2_{O,\mathbb{G}_m}}{\sum_{i=1}^{M} \sigma^2_{O,\mathbb{G}_i}}. \tag{3.19}$$

A large value of $\eta(\mathbb{G}_m)$ signifies that the observable is sensitive to changes in that group of LECs.

As an example of partial variances, I will return to the neutron-proton total elastic cross section already studied in section 3.4. I will here consider the same N3LOsim potential and group the LECs according to the chiral order to which they belong. I calculate the partial variances as a function of the scattering energy, $\eta(\mathbb{G}_m, T_{\text{lab}})$, for these groups. To more clearly show the energy dependence, I have normalized the partial variances as

$$\hat{\eta}(\mathbb{G}_m, T_{\text{lab}}) \equiv \frac{\eta(\mathbb{G}_m, T_{\text{lab}})}{\int_0^{T_{\text{lab}}^{\text{max}}} \eta(\mathbb{G}_m, t)\,\mathrm{d}t}, \tag{3.20}$$

where $T_{\text{lab}}^{\text{max}} = 350\,\text{MeV}$. The result is shown in figure 3.5. The LO LECs of the N3LOsim interaction show a strongly decreasing sensitivity as a function of increasing energy. This indicates that those LECs have a larger relative impact at low energies. The NLO LECs have a mostly constant relative impact with a small peak around 120 MeV. Also the N3LO LECs display a mostly flat behavior with a small increase at the highest energies. N2LO, consisting only of pion-nucleon and three-nucleon LECs, have a more complex form. Overall, there are only small tendencies that higher order LECs have a larger impact at higher energies, in contrast to what was indicated by the auto-correlation analysis presented in section 3.4.

The two examples on sensitivity analyses presented in this section highlights what kind of information that can be gained from studying statistical properties of the interactions. Further work on sensitivities could yield additional valuable insights.

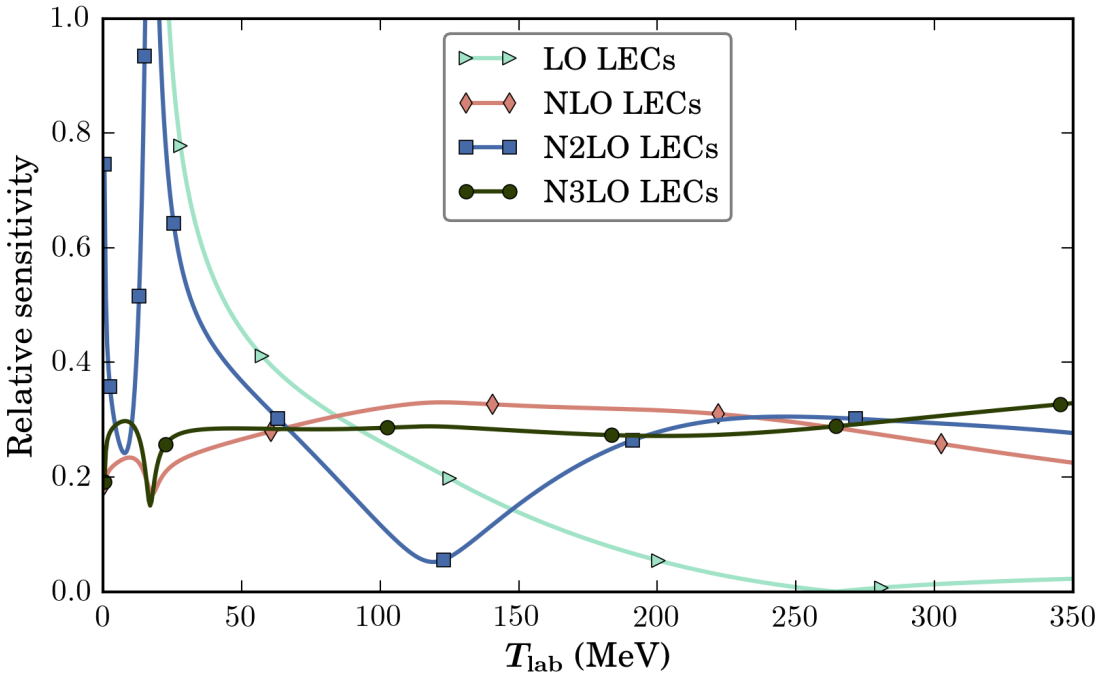

Figure 3.5: Normalized partial variances of LECs as a function of laboratory kinetic energy for the total cross section for neutron-proton elastic scattering. The data shown in the figure is for the N3LOsim interaction presented in paper D. The sensitivity is shown separately for LECs entering at different orders in the chiral expansion. The curves indicates what energies the different groups of LECs are sensitive to. As expected, the LO LECs are most sensitive to the low-energy region. For the other orders there is no clear indication that higher-order LECs are more sensitive to high-energy observables.

Chapter 4

Global analysis

In chapter 3, I described the quality of individual interactions as well as their statistical and systematic uncertainties. Another way to estimate systematic uncertainties and to also find general correlations between predictions, is to look at a set of chiral interactions that are fitted in slightly different manners. With such an approach, it is possible to see which results are accidental and which results that are robust to changes in the model. In section 4.1 I describe how we construct such families of interactions while in section 4.2 I show some results.

4.1 Family of potentials

As mentioned in chapter 2, the interactions are regulated using a cut-off parameter Λ. This is necessary to cut off the high-momentum part of the interaction. In principle, the predictions of the model should be independent of the choice of Λ within a reasonable range, with the values of the LECs changing to keep theoretical values of observables independent of Λ. However, theoretical predictions do exhibit a dependence on Λ The obtained spread in predictions can be interpreted as an indication of the uncertainty in the model.

Furthermore, there is no single correct set of experimental data to use for fitting chiral interactions. Interactions optimized to different sets of experimental data will generally yield slightly different predictions. As long as all sets of data are enough to constrain all directions in the space of LECs, this spread in predictions is also an indication of the model uncertainty.

In papers B and D we combine the two above mentioned methods for varying the interaction slightly — different values of Λ and different sets of experimental data — to construct families of interactions at order LO through N3LO. The value of Λ is varied in seven steps between 450 and 600 MeV. The lower limit was chosen such that only the high-energy part of the interaction is affected. An upper limit of $\Lambda = 600$ MeV was chosen to stay well below the break-down scale of χEFT. Fitting to different sets of experimental data was achieved by varying the upper limit for the kinetic energy for included nucleon-nucleon scattering data, $T_{\text{lab}}^{\text{max}}$. This value was varied between 125 and 290 MeV. In total, the family at each order consists of 42 interactions.

In paper B we employ this family of interactions at N2LO to approximate the model uncertainty in the ground-state binding energies of helium-4 and oxygen-16, as shown in figure B.11. For helium-4 the spread is almost 2 MeV, or 0.5 MeV per nucleon, which is significantly larger than all other sources of uncertainty. This indicates that it would be beneficial to include an estimate for the model uncertainty for the bound-state properties in the fitting procedure, as is done for the scattering observables. For oxygen-16 the spread is instead 35 MeV, or around 2 MeV per nucleon. This is a considerable increase, indicating that heavier systems are not well constrained by our interactions, which are fitted only to experimental data for two- and three-nucleon systems. The issue is not primarily that the interactions need to be better constrained in a statistical sense, i.e. smaller experimental uncertainties for the included data would not help, as the model uncertainties seem to be much larger. Also, for oxygen-16 the interactions consistently produce too weak binding. In fact, the energies of oxygen-16 as provided by the coupled cluster calculations are below the 4α breakup. This can be either due to an underestimation of the model uncertainty, or it could be that the minima we have found are incompatible with a proper description of heavier systems. If the first explanation would be the correct one, it would imply that the model uncertainties for heavy systems are so large that the theory has essentially no predictive power for such systems. If the discrepancy in oxygen-16 instead is due to incompatible minima, i.e. that important experimental observables are missing from the fit, then the predictions should be able to improve. This was investigated in reference [53], where a chiral interaction at N2LO was constructed with binding energies and radii from oxygen isotopes and carbon-14 included in the fitting procedure. This resulted in a much improved description of heavier systems [54], indicating that such observables

are needed to inform the model of such physics. However, the systematic uncertainties are difficult to assess.

As a side note, it should be pointed out that if the interactions I have developed in papers B and D would be refitted with experimental data for heavier systems added to the chi-squared function, that would result in a worse description of the $A = 2, 3$ data already included. This is true for any new data added to the fitting procedure. The explanation is that the minima I have found are the ones that best describe the already included $A = 2, 3$ data. The addition of new data will result in new values for the LECs — values that are not optimal when considering only the $A = 2, 3$ data. This in turn implies that we have underestimated the model uncertainty for the scattering data, since the size of this uncertainty was tuned so as to obtain a chi-squared per datum value of one. I.e., an increased chi-squared value would force the estimated model uncertainty to be larger.

When constructing a family of interactions at N3LO, it turns out that varying the included experimental data by lowering $T_{\text{lab}}^{\text{max}}$ results in poorly fitted interactions. The reason is that without all the scattering data up to 290 MeV the interaction at this order is not well enough constrained. With more LECs, more data are required for a well-constrained fit. As demonstrated already in figure 3.3, experimental scattering data are less and less correlated at higher orders. This indicates that the scattering data at different energies help constrain different directions in the space of LECs.

The lack of data for the fits at N3LO is also the reason to why we were able to find around a hundred different local minima, as mentioned in section 3.1. Since all these minima describe the included data well, they can also be used as a family of interactions to study uncertainties in the model. For example, it is possible to gauge what range of values for observables not included in the fit that are compatible with a good description of all the data included in the fitting. For example, employing the 104 interactions obtained in optimization step (V) in paper D I obtain an alarming range of values already for the helium-4 binding energy. It should be noted, however, that some of these interactions could be discarded due to other considerations. In paper B we mention that the Wigner symmetry should be fulfilled [55], which is not the case for all of the N3LO interactions. This symmetry implies that $\tilde{C}_{^1S_0}$ should be approximately equal to $\tilde{C}_{^3S_1}$.

4.2 Global correlations

With the families of interactions at all orders up to N3LO, it is possible to study uncertainties in the model, as I did in the previous section, and also correlations. Instead of starting with the statistical variations as in section 3.4, a correlation is here obtained from a linear regression of the predictions of two observables. This is a method for exploring correlations that are valid globally across different LEC values and different values of the regulator cutoff Λ.

The Tjon line [56] describes a linear relation between the theoretical predictions of the binding energies of triton and helium-4 when excluding the three-body force from the calculations. This relation can be investigated with the families of potentials described in section 4.1. The predictions are shown in figure 4.1 and are seen to approximately fall on a line. With the

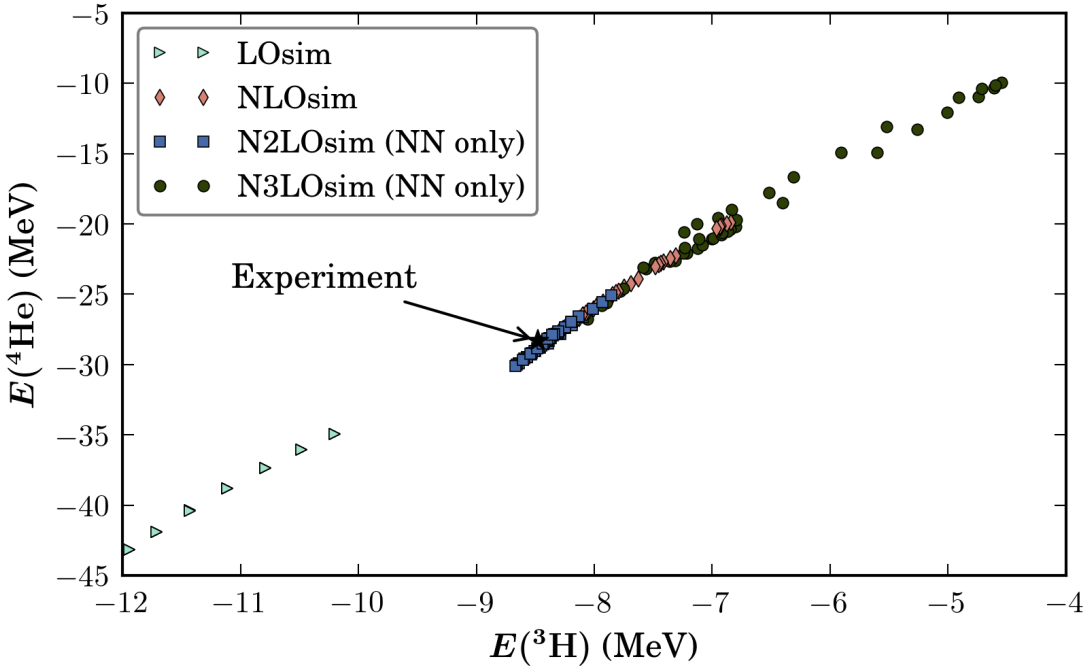

Figure 4.1: Theoretical predictions for the binding energies of triton and helium-4 using only the two-nucleon force, i.e. excluding the three-nucleon force. The results are for the families of interactions presented in section 4.1. A linear relationship is obtained, called the Tjon line.

three-nucleon force included, all interactions at the orders N2LO and N3LO

reproduce the triton binding energy within the employed uncertainty. From the figure it is then clear that for our fits at N3LO the three-nucleon force needs to contribute more to the binding energy compared to at N2LO. This contradicts that the three-nucleon force at N3LO should be a small correction to N2LO.

It is also instructive to study the correlation matrix and autocorrelation function presented in section 3.4 from a global perspective. With such an analysis one can gauge the flexibility of the interactions at various orders. I will here examine the total elastic cross section for neutron-proton scattering, the same observable as in section 3.4. The correlations obtained from the family of 42 N3LO interactions, where both Λ and $T_{\mathrm{lab}}^{\mathrm{max}}$ are varied, are shown in figure 4.2 and can be compared with figure 3.2. The correlation matrices

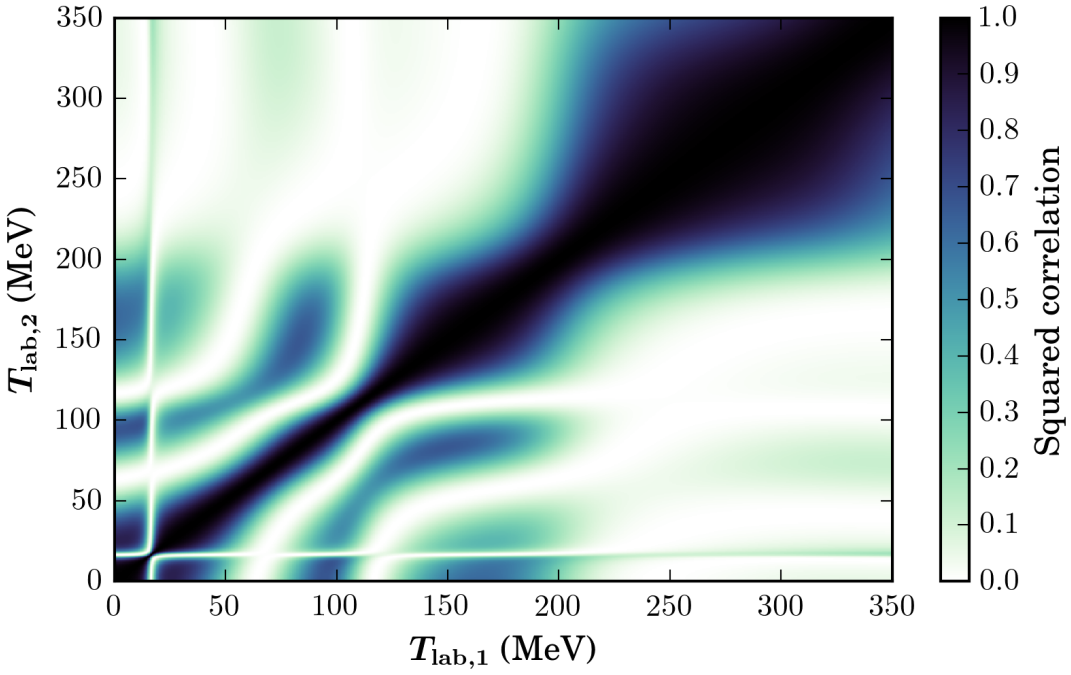

Figure 4.2: Global correlations for the theoretical predictions of the neutron-proton total elastic scattering cross section as a function of the laboratory kinetic energy for a family of 42 N3LOsim potentials. Shown as a gradient is the correlation squared, with darker tones signifying stronger correlations.

are similar, although the global case contain some isolated regions of high correlation that are not present in the statistical case. However, the general trend of decreasing correlation with increasing energy difference is seen also

in the global case.

The autocorrelation function, defined in section 3.4, applied to the correlations for the theoretical predictions of the family of interactions, is shown in figure 4.3. The figure can be compared with figure 3.3, where statistical correlations are shown. Similar trends are seen in the global case as

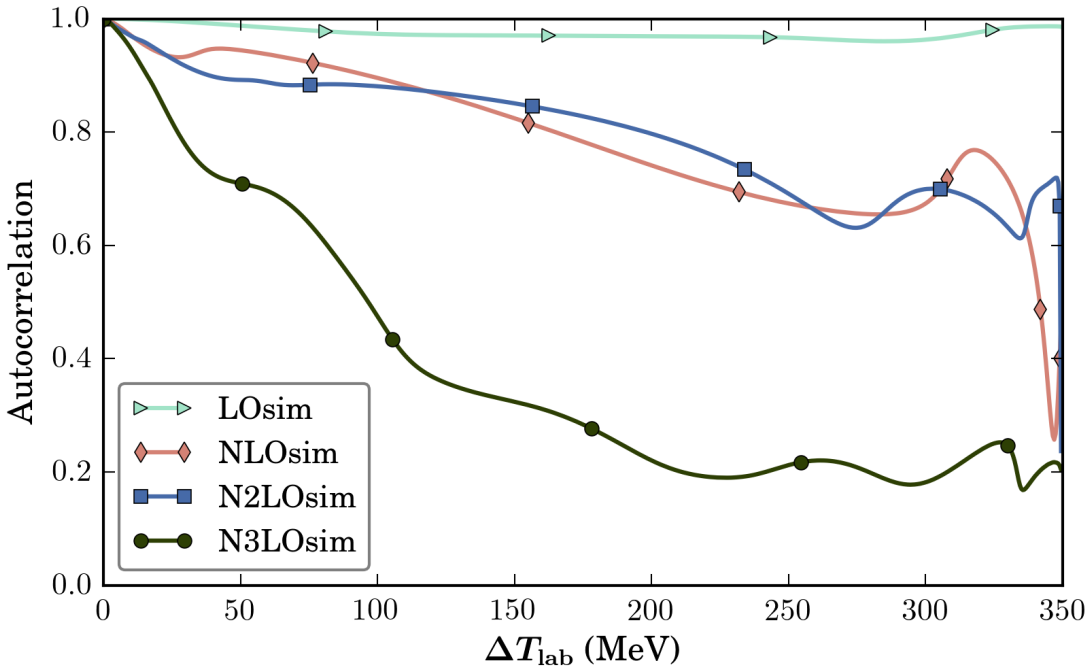

Figure 4.3: Autocorrelation function (see (3.9)*) for the global correlations of the theoretical predictions of the neutron-proton total elastic scattering cross section as a function of the laboratory kinetic energy for the families of potentials presented in section 4.1. The correlation is seen to generally decrease with increased energy difference.*

in the statistical correlations, although the NLO and N2LO autocorrelations are more similar in the former case. Overall, the autocorrelation for this observable indicates that the model has a larger degree of flexibility at higher orders.

With the families of interactions in place, many other global trends and correlations should be studied also, which is an important point in my outlook.

Chapter 5

Conclusion and outlook

Two important aspects of a physical model — uncertainty estimations and predictive power — were mentioned already in the introduction to this extended summary. Having these aspects in mind a comprehensive analysis of how to quantify such uncertainties in the theoretical calculations using χEFT was presented and discussed in chapters 3 and 4. Here, in this final chapter, I point out the most important conclusions of my work and also discuss possible future avenues to pursue.

My thesis work can be divided into the following three areas:

1. Development of algorithms and code for numerical calculations:
   - My implementation for evaluating potential matrix elements for the two-nucleon interaction currently handles χEFT potentials up to and including N3LO; is flexible and easy to extend; is fast compared to other steps in the calculations, and also provides accurate derivatives with respect to the LECs.
   - I have improved the efficiency of the calculation of nuclear two-body scattering observables and NCSM observables.
   - For the evaluation of derivatives using automatic differentiation I have implemented efficient algorithms for the inversion and diagonalization of a matrix.
   - My methods for statistical error propagation are capable of utilizing both first- and second-order derivatives for improved uncertainty estimations.

2. Optimization of χEFT interactions:
   - I have used both phase shifts, which are inferred and model-dependent quantities, and experimental observables to constrain the LECs of χEFT interactions up to and including the fourth order in the chiral expansion.
   - In particular, I have been leading the development of a simultaneous fitting procedure, in which all the LECs of the interaction are determined in one single fit to experimental data. This is a demanding approach, involving a non-linear least-squares minimization of up to 41 parameters to a heterogeneous set of data consisting of two-nucleon and pion-nucleon scattering observables as well as bound-state energies, radii and half-life for two-, three- and sometimes also four-nucleon systems.
   - For two-body scattering observables I developed a method to estimate the model uncertainty, which can be included directly in the chi-squared minimization. This improves the fitting procedure and removes an ambiguity in the choice of fit data.
3. Analysis of the resulting interactions:
   - I examined the quality of the resulting interactions by inspecting properties of the chi-squared function, for example distribution of residuals and partial chi-squared values to probe the accuracy of the model as a function of scattering energy.
   - I calculated statistical and systematic uncertainties as a means to probe the expected precision and accuracy of the model as well as to determine the convergence of χEFT with respect to different chiral orders.
   - To further check the correctness of the statistical uncertainties I implemented and tested the Lagrange multiplier method for obtaining uncertainties. I found that such a method is superior when the quadratic approximation of the chi-squared surface around the minimum does not hold.
   - I studied local and global correlations to further analyze the interaction and the data.

The computational implementation is flexible and allows for arbitrary diagrams up to N3LO in the chiral expansion to be included in the

calculations. This makes it possible to perform calculations at mixed orders, e.g. including only some diagrams from a higher order or excluding a particular diagram. At the same time, different regulators and different schemes for defining the non-relativistic potential can be employed. With the developed implementation I was able to perform extensive searches in the space of LECs for good fits to experimental data. This is an important step in non-linear minimizations as sometimes there are several local minima, as demonstrated in section 3.1. The efficiency of the implementation also enabled me to include computationally intensive observables such as the binding energy and radius of helium-4 in the chi-squared function.

By including an estimate of the model uncertainty already in the fitting procedure I was able to fit to a larger set of experimental data with a reduced risk of overfitting. Without the model uncertainty, the minimization routine will fine tune the interaction to reproduce data that are not expected to be accurately described by the theory. On the other hand, as discussed in section 2.4, when the model uncertainty is the dominant source of uncertainty, correlations are induced between the residuals in the chi-squared function. These correlations could also cause overfitting since the chi-squared function I use assumes uncorrelated residuals.

I was also able to perform simultaneous fits of all LECs up to a given order. This was seen to improve the description of experimental data in the sense of a lower obtained chi-squared value, and reduced the number of local minima. This approach was made possible through my development of an efficient framework for theoretical calculations. The simultaneous minimization also improved the subsequent statistical analysis since correlations between all LECs are obtained.

When interactions had been fitted to experimental data, I could begin the investigation of the central themes; uncertainties and predictive power, as well as the convergence of χEFT. With the developed simultaneous fitting procedure, statistical uncertainties were seen to be small compared to systematic uncertainties in the model. The convergence of χEFT is clearly seen in the scattering data. For example, figure B.9 show that the predictions at higher orders have smaller uncertainties than at lower orders. The correlations and sensitivity analyses presented in sections 3.4 and 3.5 make it possible to probe statistical properties of χEFT. I examined in particular the correlations between scattering observables at different kinetic energies. I found that the correlation decreases with increasing energy difference and also with increasing order. This indicates that as the order increases, the

different energy regions become sensitive to different parts of the interaction. This is consistent with the expectation that higher-order contributions should mainly affect the higher-energy observables. I also outlined possible methods for performing sensitivity analyses. With such analyses it is possible to investigate which data that affect which LECs and to define partial variances to find the contribution to the statistical uncertainty from different LECs.

In section 4.1 I presented families of chiral interactions, whose members were fitted using different values for the regulator cut-off parameter Λ and/or different truncations of the experimental data. This allowed to probe systematic uncertainties and global correlations in the model. In section 4.2 I used these families to estimate the model uncertainty for bound-state observables and to study correlations such as the Tjon line. For the bound-state observables the spread in predictions was seen to be significantly larger than other sources of uncertainties, see e.g. figure B.11. This indicates that the model uncertainty is large for these observables.

The computational and statistical tools that I have developed pave the way for research in many other directions. As indicated in section 3.2, it is possible to further investigate an improved form of the model uncertainty with the help of the chi-squared function and its properties. For example, in section 3.1 I concluded that the low-energy form of the model uncertainty can be improved and in figure 3.1 I illustrated that the model uncertainty for the high-energy nucleon-nucleon scattering data is estimated to be too large. A related issue is the model uncertainty for the bound-state observables. I have not included this uncertainty in the minimization due to the difficulty of estimating it. However, in papers B and D it was indicated that the model uncertainty for these observables are larger than both the experimental uncertainty and the uncertainty in the method of calculation. It would therefore be desirable to include the model uncertainty in the fitting procedure. There are also ongoing efforts to use a Bayesian framework to calculate statistical and systematic uncertainties [57, 58], which has the potential to further improve the uncertainty estimates. The success of the method is contingent on an efficient implementation for calculating observables. Therefore, the framework I have helped develop can serve as a key component in the implementation of a Bayesian analysis.

With my efficient implementation for two-nucleon matrix element calculations, moving to higher orders in the chiral expansion for the two-nucleon force is not an issue from a computational point of view. In fact, terms in the chiral expansion for the two-nucleon sector have already been derived

up to N5LO [27, 59]. However, many-nucleon forces such as the four-body forces are still computationally challenging to include in theoretical calculations. The effective field theory I have used includes only pions and nucleons. Instead of moving to higher orders, it is possible to improve the theory by including more explicit degrees of freedom. The Δ-excitation of the nucleon has been identified as the most salient feature to include and work in deriving expressions for the diagrams is under way [60]. Implementing the Δ-full theory is possible in our computing framework. Another avenue made possible by the flexible and efficient implementation is to investigate the correctness of the power counting. It has been argued that additional counter terms, i.e. contact interaction terms, are needed at lower orders [16–18]. This can be investigated in a non-perturbative setting using our tool set.

In section 3.3 I highlighted that improved statistical methods need to be employed in the analysis of the N3LOsim potentials since the chi-squared surface around the minimum is not quadratic. Instead, fourth-order terms dominate in some directions, which is due to large uncertainties in the LECs. To avoid these large uncertainties, experimental data that are sensitive to the corresponding directions need to be included in the fitting procedure. There are two natural directions, or philosophies, that could be followed: Either one can include more experimental data for systems with $A \lesssim 4$ — i.e. adopting a bottom-up approach with respect to the number of nucleons — or one can include observables for larger systems — i.e. embracing low-energy observables regardless of system size. The first direction is motivated by that in χEFT up to N3LO, only two-, three- and four-nucleon forces exist and therefore such observables should be sufficient for constraining the theory. In this approach, the inclusion of three-body scattering data would be a natural step forward. Methods for calculating such observables have been developed [61–63]. Just as for two-nucleon scattering there are many experimental results for three-nucleon scattering, see e.g. reference [64] and references therein. A possible benefit of the second direction is that heavy systems could contain physics that cannot be captured by the lighter systems, such as the nuclear saturation density [53, 65].

To conclude, the simultaneous fitting method for constraining χEFT has produced improved interactions with better known properties and the developed framework is a valuable tool for future research.

Chapter 6

Summary of papers

In paper A we constructed an N2LO χEFT potential where the LECs were fitted to two-nucleon scattering data using the POUNDerS algorithm [66]. We then performed a statistical analysis to obtain uncertainties for the LECs. These uncertainties were propagated to other observables such as deuteron properties. A sensitivity analysis for selected deuteron properties was also performed.

In paper B we improved upon the results presented in paper A. We constructed LO, NLO and N2LO potentials using a simultaneous fit to pion-nucleon, two-nucleon and few-nucleon experimental data. We also included an estimate of the inherent model uncertainty, which improved the fitting procedure and allowed us to include more data. We performed a subsequent statistical analysis where we propagated statistical errors to selected bound-state properties in nuclei up to ^{4}He and ^{16}O. The systematic uncertainty in the model was further investigated using a family of 42 interactions constructed in slightly different ways. The spread in the predictions of this family was used to estimate the uncertainty in the model for bound states. It was found that the spread increases rapidly with increasing number of nucleons.

In paper D we extended the analysis performed in paper B to N3LO. We use the same experimental data to constrain the model and the same form for the model uncertainty. With the additional diagrams in the interaction at N3LO and a total of 41 LECs, we find that the experimental data used is insufficient to uniquely determine the values of the LECs. We also find that the statistical variations in the LECs are not well reproduced using the approximations from paper B. Instead we adopted some of the methods

described in paper C.

In paper C the statistical uncertainties were analyzed further in order to verify their soundness. Several methods for calculating and propagating statistical uncertainties were compared, with a focus on the Lagrange multiplier method. I compared approximations used in these methods and their impact on the statistical uncertainties. One of the conclusions is that with large statistical uncertainties the Lagrange multiplier method provides more accurate results.

Bibliography

[1] G. Baym, H. A. Bethe, and C. J. Pethick, "Neutron star matter," *Nucl. Phys. A* **175** (1971) 225 – 271.

[2] F. D. Mackie and G. Baym, "Compressible liquid drop nuclear model and mass formula," *Nucl. Phys. A* **285** (1977) 332 – 348.

[3] A. S. Kronfeld and C. Quigg, "Resource Letter QCD-1: Quantum chromodynamics," *American Journal of Physics* **78** (2010) 1081–1116.

[4] NPLQCD Collaboration, K. Orginos, A. Parreño, M. J. Savage, S. R. Beane, E. Chang, and W. Detmold, "Two nucleon systems at $m_\pi \sim 450$ MeV from lattice QCD," *Phys. Rev. D* **92** (2015) 114512.

[5] J. Green, M. Engelhardt, S. Krieg, J. Negele, A. Pochinsky, and S. Syritsyn, "Nucleon structure from Lattice QCD using a nearly physical pion mass," *Phys. Lett. B* **734** (2014) 290 – 295.

[6] S. Aoki, "Nucleon-nucleon interactions via Lattice QCD: Methodology," *Eur. Phys. J. A* **49** (2013) 81.

[7] H. Yukawa, "On the Interaction of Elementary Particles," *Proc. Phys. Math. Soc. Japan* **17** (1935) .

[8] R. Machleidt, "High-precision, charge-dependent Bonn nucleon-nucleon potential," *Phys. Rev. C* **63** (2001) 024001.

[9] R. N. Pérez, J. E. Amaro, and E. R. Arriola, "Coarse-grained potential analysis of neutron-proton and proton-proton scattering below the pion production threshold," *Phys. Rev. C* **88** (2013) 064002.

[10] N. Kalantar-Nayestanaki, E. Epelbaum, J. G. Messchendorp, and A. Nogga, "Signatures of three-nucleon interactions in few-nucleon systems," *Reports on Progress in Physics* **75** (2012) 016301.

[11] G. Box and N. Draper, *Empirical model-building and response surfaces*. Wiley series in probability and mathematical statistics: Applied probability and statistics. Wiley (1987). `http://dl.acm.org/citation.cfm?id=17317`.

[12] J. Dobaczewski, W. Nazarewicz, and P.-G. Reinhard, "Error estimates of theoretical models: a guide," *J. Phys. G* **41** (2014) 074001.

[13] S. Weinberg, "Phenomenological Lagrangians," *Physica A* **96** (1979) 327 – 340.

[14] R. Machleidt and D. Entem, "Chiral effective field theory and nuclear forces," *Phys. Rep.* **503** (2011) 1 – 75.

[15] S. Weinberg, "Nuclear forces from chiral lagrangians," *Phys. Lett. B* **251** (1990) 288 – 292.

[16] A. Nogga, R. G. E. Timmermans, and U. v. Kolck, "Renormalization of one-pion exchange and power counting," *Phys. Rev. C* **72** (2005) 054006.

[17] B. Long and C.-J. Yang, "Renormalizing chiral nuclear forces: Triplet channels," *Phys. Rev. C* **85** (2012) 034002.

[18] A. Kievsky, M. Viviani, M. Gattobigio, and L. Girlanda, "Implications of Efimov physics for the description of three and four nucleons in chiral effective field theory," *Phys. Rev. C* **95** (2017) 024001.

[19] S. Weinberg, "Effective chiral lagrangians for nucleon-pion interactions and nuclear forces," *Nucl. Phys. B* **363** (1991) 3 – 18.

[20] E. Epelbaum, W. Glöckle, and U.-G. Meißner, "The two-nucleon system at next-to-next-to-next-to-leading order," *Nucl. Phys. A* **747** (2005) 362 – 424.

[21] E. Epelbaum, "Few-nucleon forces and systems in chiral effective field theory," *Prog. Part. Nucl. Phys.* **57** (2006) 654 – 741.

[22] E. Epelbaum, A. Nogga, W. Glöckle, H. Kamada, U.-G. Meißner, and H. Witała, "Three-nucleon forces from chiral effective field theory," *Phys. Rev. C* **66** (2002) 064001.

[23] K. Hebeler, H. Krebs, E. Epelbaum, J. Golak, and R. Skibiński, "Efficient calculation of chiral three-nucleon forces up to N^{3}LO for *ab initio* studies," *Phys. Rev. C* **91** (2015) 044001.

[24] N. Fettes, U.-G. Meißner, and S. Steininger, "Pion-nucleon scattering in chiral perturbation theory (I): Isospin-symmetric case," *Nucl. Phys. A* **640** (1998) 199 – 234.

[25] K. Wendt, B. Carlsson, and A. Ekström, "Uncertainty Quantification of the Pion-Nucleon Low-Energy Coupling Constants up to Fourth Order in Chiral Perturbation Theory," `arXiv:1410.0646 [nucl-th]`.

[26] E. Epelbaum and U.-G. Meißner, "On the Renormalization of the One–Pion Exchange Potential and the Consistency of Weinberg's Power Counting," *Few-Body Syst.* **54** (2013) 2175–2190.

[27] D. R. Entem, N. Kaiser, R. Machleidt, and Y. Nosyk, "Peripheral nucleon-nucleon scattering at fifth order of chiral perturbation theory," *Phys. Rev. C* **91** (2015) 014002.

[28] K. Erkelenz, R. Alzetta, and K. Holinde, "Momentum space calculations and helicity formalism in nuclear physics," *Nucl. Phys. A* **176** (1971) 413 – 432.

[29] Bystricky, J., Lehar, F., and Winternitz, P., "Formalism of nucleon-nucleon elastic scattering experiments," *J. Phys. France* **39** (1978) 1–32.

[30] La France, P. and Winternitz, P., "Scattering formalism for nonidentical spinor particles," *J. Phys. France* **41** (1980) 1391–1417.

[31] H. Krebs, A. Gasparyan, and E. Epelbaum, "Chiral three-nucleon force at N^{4}LO: Longest-range contributions," *Phys. Rev. C* **85** (2012) 054006.

[32] B. Tromborg, S. Waldenstrøm, and I. Øverbø, "Electromagnetic corrections in hadron scattering, with application to πN $\to$ πN," *Helv. Phys. Acta* **51** (1978) 584.

[33] B. Tromborg and J. Hamilton, "Electromagnetic corrections to hadron-hadron scattering," *Nucl. Phys. B* **76** (1974) 483 – 540.

[34] B. Tromborg, S. Waldenstrøm, and I. Øverbø, "Electromagnetic corrections to πN scattering," *Phys. Rev. D* **15** (1977) 725–729.

[35] D. Bugg, "Coulomb corrections to πN elastic scattering," *Nucl. Phys. B* **58** (1973) 397 – 407.

[36] P. Navrátil, G. P. Kamuntavičius, and B. R. Barrett, "Few-nucleon systems in a translationally invariant harmonic oscillator basis," *Phys. Rev. C* **61** (2000) 044001.

[37] E. Anderson, Z. Bai, C. Bischof, S. Blackford, J. Demmel, J. Dongarra, J. Du Croz, A. Greenbaum *et al.*, *LAPACK Users' Guide*. Society for Industrial and Applied Mathematics, Philadelphia, PA, third ed. (1999). `http://www.netlib.org/lapack/lug`.

[38] D. Gazit, S. Quaglioni, and P. Navrátil, "Three-Nucleon Low-Energy Constants from the Consistency of Interactions and Currents in Chiral Effective Field Theory," *Phys. Rev. Lett.* **103** (2009) 102502.

[39] R. A. Arndt, I. I. Strakovsky, and R. L. Workman, *SAID, Scattering Analysis Interactive Dial-in computer facility, George Washington University (formerly Virginia Polytechnic Institute), solution SM99 (Summer 1999); for more information see, e.g., R. A. Arndt, I. I. Strakovsky, and R. L. Workman, Phys. Rev. C* **50***, 2731 (1994).* (1999).

[40] V. G. J. Stoks, R. A. M. Klomp, M. C. M. Rentmeester, and J. J. de Swart, "Partial-wave analysis of all nucleon-nucleon scattering data below 350 MeV," *Phys. Rev. C* **48** (1993) 792–815.

[41] J. R. Bergervoet, P. C. van Campen, R. A. M. Klomp, J.-L. de Kok, T. A. Rijken, V. G. J. Stoks, and J. J. de Swart, "Phase shift analysis of all proton-proton scattering data below T_{lab}=350 MeV," *Phys. Rev. C* **41** (1990) 1435–1452.

[42] R. Navarro Pérez, J. E. Amaro, and E. Ruiz Arriola, "Partial-wave analysis of nucleon-nucleon scattering below the pion-production threshold," *Phys. Rev. C* **88** (2013) 024002.

[43] R. Navarro Pérez, J. E. Amaro, and E. R. Arriola, "Erratum: Coarse-grained potential analysis of neutron-proton and proton-proton scattering below the pion production threshold [Phys. Rev. C **88** , 064002 (2013)]," *Phys. Rev. C* **91** (2015) 029901.

[44] R. L. Workman, R. A. Arndt, W. J. Briscoe, M. W. Paris, and I. I. Strakovsky, "Parameterization dependence of T-matrix poles and eigenphases from a fit to πN elastic scattering data," *Phys. Rev. C* **86** (2012) 035202.

[45] E. Epelbaum, H. Krebs, and U.-G. Meißner, "Improved chiral nucleon-nucleon potential up to next-to-next-to-next-to-leading order," *Eur. Phys. J. A* **51** (2015) 53.

[46] E. Epelbaum, H. Krebs, and U.-G. Meißner, "Precision Nucleon-Nucleon Potential at Fifth Order in the Chiral Expansion," *Phys. Rev. Lett.* **115** (2015) 122301.

[47] LENPIC Collaboration, S. Binder, A. Calci, E. Epelbaum, R. J. Furnstahl, J. Golak, K. Hebeler, H. Kamada, H. Krebs *et al.*, "Few-nucleon systems with state-of-the-art chiral nucleon-nucleon forces," *Phys. Rev. C* **93** (2016) 044002.

[48] S. M. Wild, J. Sarich, and N. Schunck, "Derivative-free optimization for parameter estimation in computational nuclear physics," *ArXiv e-prints* (2014) , `arXiv:1406.5464 [physics.comp-ph]`.

[49] D. W. Marquardt, "An Algorithm for Least-Squares Estimation of Nonlinear Parameters," *SIAM J. Appl. Math.* **11** (1963) 431–441.

[50] D. Cline and P. Lesser, "Error estimation in non-linear least squares analysis of data," *Nucl. Instr. Meth.* **82** (1970) 291 – 293.

[51] R. T. Birge, "The Calculation of Errors by the Method of Least Squares," *Phys. Rev.* **40** (1932) 207–227.

[52] S. Bogner, R. Furnstahl, R. Perry, and A. Schwenk, "Are low-energy nuclear observables sensitive to high-energy phase shifts?," *Phys. Lett. B* **649** (2007) 488 – 493.

[53] A. Ekström, G. R. Jansen, K. A. Wendt, G. Hagen, T. Papenbrock, B. D. Carlsson, C. Forssén, M. Hjorth-Jensen *et al.*, "Accurate nuclear radii and binding energies from a chiral interaction," *Phys. Rev. C* **91** (2015) 051301.

[54] G. Hagen, A. Ekström, C. Forssén, G. R. Jansen, W. Nazarewicz, T. Papenbrock, K. A. Wendt, S. Bacca *et al.*, "Neutron and weak-charge distributions of the 48Ca nucleus," *Nature Phys.* **12** (2016) 186–190. Article.

[55] T. Mehen, I. W. Stewart, and M. B. Wise, "Wigner Symmetry in the Limit of Large Scattering Lengths," *Phys. Rev. Lett.* **83** (1999) 931–934.

[56] J. Tjon, "Bound states of 4He with local interactions," *Phys. Lett. B* **56** (1975) 217 – 220.

[57] R. J. Furnstahl, D. R. Phillips, and S. Wesolowski, "A recipe for EFT uncertainty quantification in nuclear physics," *J. Phys. G* **42** (2015) 034028.

[58] R. J. Furnstahl, N. Klco, D. R. Phillips, and S. Wesolowski, "Quantifying truncation errors in effective field theory," *Phys. Rev. C* **92** (2015) 024005.

[59] D. R. Entem, N. Kaiser, R. Machleidt, and Y. Nosyk, "Dominant contributions to the nucleon-nucleon interaction at sixth order of chiral perturbation theory," *Phys. Rev. C* **92** (2015) 064001.

[60] H. Krebs, E. Epelbaum, and U. G. Meißner, "Nuclear forces with Δ excitations up to next-to-next-to-leading order, part I: Peripheral nucleon-nucleon waves," *Eur. Phys. J. A* **32** (2007) 127–137.

[61] L. E. Marcucci, A. Kievsky, L. Girlanda, S. Rosati, and M. Viviani, "$N-d$ elastic scattering using the hyperspherical harmonics approach with realistic local and nonlocal interactions," *Phys. Rev. C* **80** (2009) 034003.

[62] A. Deltuva, "Momentum-space calculation of proton-deuteron scattering including Coulomb and irreducible three-nucleon forces," *Phys. Rev. C* **80** (2009) 064002.

[63] H. Witała, J. Golak, R. Skibiński, and K. Topolnicki, "Calculations of three-nucleon reactions with N 3 LO chiral forces: achievements and challenges," *J. Phys. G* **41** (2014) 094011.

[64] A. Ramazani-Moghaddam-Arani, H. R. Amir-Ahmadi, A. D. Bacher, C. D. Bailey, A. Biegun, M. Eslami-Kalantari, I. Gašparić, L. Joulaeizadeh *et al.*, "Elastic proton-deuteron scattering at intermediate energies," *Phys. Rev. C* **78** (2008) 014006.

[65] C. Drischler, K. Hebeler, and A. Schwenk, "Asymmetric nuclear matter based on chiral two- and three-nucleon interactions," *Phys. Rev. C* **93** (2016) 054314.

[66] S. Wild, "Solving derivative-free nonlinear least squares with POUNDERS," *Preprint ANL/MCS-P5120-0414, Argonne Nat. Lab., Argonne, IL* (2014) . `http://www.mcs.anl.gov/publication/solving-derivative-free-nonlinear-least-squares-pounders`.